Thesis for the degree of Doctor of Philosophy

Fast ions and turbulent particle transport in tokamaks

Frida Eriksson

CHALMERS

Department of Space, Earth and Environment
Chalmers University of Technology
Göteborg, Sweden 2019

Fast ions and turbulent particle transport in tokamaks
FRIDA ERIKSSON

ISBN 978-91-7905-136-5
Doktorsavhandlingar vid Chalmers tekniska högskola
Ny serie nr 4603
ISSN 0346-718X

Department of Space, Earth and Environment
Astronomy and Plasma Physics
Chalmers University of Technology
SE-412 96 Göteborg, Sweden
Telephone +46 (0)31-772 1000

Chalmers Reproservice
Göteborg, Sweden 2019

Fast ions and turbulent particle transport in tokamaks

Frida Eriksson
Department of Space, Earth and Environment
Chalmers University of Technology
SE-412 96 Göteborg, Sweden

Abstract

The presence of highly energetic (fast) ions, be it fusion born alpha particles or ions accelerated by auxiliary heating schemes, can affect the heating and transport of all particles in the plasma through two main mechanisms. First, fast ions may excite fast ion driven instabilities. One such example is the toroidal Alfvén eigenmode (TAE) that can be excited by super Alfvénic ions as they slow down due to friction-like collisions with the background plasma and eventually hit the wave-particle resonances. In addition, the fast ions may influence the turbulent transport, driven by temperature and density gradients in the background plasma. The turbulent particle transport, together with particle sources, determines the peaking of the density profile in fusion devices which in turn affect the fusion power generated.

In this thesis we employ a simple one-dimensional electrostatic "bump-on-tail" model to qualitatively describe fast ion driven TAEs whose signals exhibit frequency sweeping. The frequency sweeping is tied to the formation and evolution of phase space structures known as holes and clumps in the non-thermal fast particle distribution. We have also made realistic simulations of particle transport driven by Ion Temperature Gradient (ITG) modes in JET plasmas heated by neutral beam injection (NBI). We study the turbulent transport using fluid, gyro-fluid and gyrokinetic simulations. Focus is on particle transport and the effect of the NBI generated fast ions on the density peaking and, finally, the influence of the NBI particle source on the density peaking.

Keywords: Fusion plasma physics, wave-particle interaction, bump-on-tail, turbulence, drift waves, numerical modelling, density peaking, NBI

List of appended papers

[A] F. Håkansson, R. M. Nyqvist and M. K. Lilley, *Directivity of Frequency Sweeping Kinetic Instabilities*, Proceedings of the 40th EPS Conference on Plasma Physics, Espoo, Finland (2013).
Contribution: Simulations with the BOT model. Close collaboration with second author on analytical calculations.

[B] F. Eriksson, R. M. Nyqvist and M. K. Lilley, *Kinetic Theory of Phase Space Plateaux in a Non-Thermal Energetic Particle Distribution*, Phys. Plasmas 22, 092126 (2015).
Contribution: Simulations with the BOT model. Close collaboration with second author on analytical calculations and writing the manuscript.

[C] M. Oberparleiter, F. Eriksson, D. Tegnered, H. Nordman and P. Strand, *Impact of fast particles and nonlocal effects on turbulent transport in plasmas with hollow density profiles*, Proceedings of the 44th EPS Conference on Plasma Physics, Belfast, Northern Ireland (2017).
Contribution: EDWM simulations and analysis thereof.

[D] F. Eriksson, M. Oberparleiter, A. Skyman, H. Nordman, P. Strand, A. Salmi, T. Tala and JET Contributors, *Impact of fast ions on density peaking in JET: fluid and gyrokinetic modelling*, Plasma Phys. Control. Fusion (2019) https://doi.org/10.1088/1361-6587/ab1e65.
Contribution: EDWM and TGLF simulations, analysis and writing of manuscript.

[E] F. Eriksson, E. Fransson, M. Oberparleiter, H. Nordman, P. Strand, A. Salmi, T. Tala and JET Contributors, *Interpretative and predictive modelling of JET collisionality scans* Submitted for Publication to Plasma Phys. Control. Fusion (2019).
Contribution: Simulations, analysis and writing of manuscript except Sec. 4.3.

Other contributions (not included)

[1.] F. Eriksson, R. M. Nyqvist and M. K. Lilley, *Kinetic Theory of Phase Space Plateaux*, Proceedings of the 42nd EPS Conference on Plasma Physics, Lisbon, Portugal (2015).

[2.] F. Eriksson, M. Oberparleiter, A. Skyman, H. Nordman, P. Strand, A. Salmi and T. Tala, *Fluid and gyrokinetic modelling of density peaking in the presence of fast particles*, TTF EU-US, San Diego, US (2018).

[3.] F. Eriksson *Modelling of density peaking in the presence of fast particles* Oral presentation at 21th Transport and Confinement Topical Group Meeting, France (2018).

[4.] T. Tala, A. Salmi, S. Mordicjk, H. Nordman, F. Eriksson *et al*, *Core density peaking experiments in JET, DIII-D and C-mod in various operational scenarious-driven by fueling or transport?* 27th IAEA Fusion Energy Conference, Ahmedabad, India (2018).

[5.] C. Maggi, H. Weisen, F. Casson, F. Auriemma, R. Lorenzini, H. Nordman, E. Delabie, F. Eriksson *et al Isotope identity experiments in JET-ILW with H and D L-mode plasmas* Accepted for Publication in Nucl. Fusion (2019).

[6.] S. Mordicjk, T. L. Rhodes, L. Zeng, A. Salmi, T. Tala, C. C. Petty, G. R. McKee, F. Eriksson *et al*, *Collisionality driven turbulent particle transport changes in DIII-D H-mode plasmas*, Currently in DIII-D internal review system (2019).

[7.] T. Tala, H. Nordman, A. Salmi, C. Bourdelle, J. Citrin, A. Czarnecka, F. Eriksson *et al*, *Density peakingin JET-Driven by fuelling or transport?* Submitted to Nucl. Fusion (2019).

[8.] F. Eriksson, *Interpretative and predictive modelling of density peaking at JET* Oral presentation at Nordic meeting, Denmark (2019).

Acknowledgments

I would like to express my sincerest gratitude to my supervisor Prof. Hans Nordman for always being available for questions and useful comments and for the continuous help and guidance in writing this thesis and the work presented within. I would also like to thank my co-workers, past and present, in particular Dr. Michael Oberparleiter and Prof. Pär Strand for providing encouragement and for answering all questions on the codes and models and Dr. Robert Nyqvist for his help my first years as a PhD student. Furthermore, I am grateful to Prof. Sergei Sharapov and Dr Lars-Göran Eriksson for general guidance and the late Prof. Mietek Lisak for introducing me to the world of plasma physics. Finally, to my wonderful family, you are my inspiration, my support and my joy.

Contents

1 Introduction **1**
- 1.1 Nuclear Fusion . . . 1
- 1.2 Turbulent Transport . . . 2
- 1.3 Theoretical Descriptions of Plasmas . . . 3
- 1.4 Heating and Fast Ions . . . 4

2 Toroidal Systems **7**
- 2.1 Magnetohydrodynamic Model . . . 8
  - 2.1.1 Equilibrium Analysis . . . 9
  - 2.1.2 Linear Stability Analysis . . . 10
- 2.2 Single Particle Motion . . . 11
- 2.3 Toroidal Instabilities . . . 13
  - 2.3.1 Cylindrical Limit . . . 13
  - 2.3.2 Toroidal Alfvén Eigenmodes . . . 14
  - 2.3.3 Energetic Particle Drive . . . 16

3 Wave-Particle Interaction **17**
- 3.1 Electrostatic Plasma Waves in a Cold Plasma . . . 18
- 3.2 Warm Plasma Waves: Linear Landau Damping . . . 19
- 3.3 Nonlinear Landau Damping . . . 21
- 3.4 Bump-on-Tail Model . . . 24
  - 3.4.1 Dissipative Bump-on-Tail Model Near Marginal Stability 26
  - 3.4.2 Dissipative Bump-on-Tail Model Far fom Marginal Stability . . . 28
- 3.5 Connection to Fast Particle Driven Instabilities in Tokamak Plasmas . . . 29

4 Turbulent Particle Transport **33**
- 4.1 Ion Temperature Gradient/Trapped Electron (ITG/TE) modes . 34
- 4.2 Transport Modelling . . . 36
  - 4.2.1 Gyrokinetic, Gyro-fluid and Fluid descriptions . . . 36
  - 4.2.2 Interpretative and Predictive Modelling . . . 36

4.3 Fast Ion Effects on ITG mode Driven Turbulence 42
4.3.1 Fast Ion Distribution Function 43

5 Brief Summary of Included Papers **47**

Bibliography **51**

Papers A–E **57**

1

Introduction

1.1 Nuclear Fusion

Throughout the world there is a steadily increasing demand for energy production, more than what the current energy sources can provide for in an economically feasible and environmentally friendly manner [1]. From an environmental point of view, there are limits to how much energy can be supplied from fossil fuels such as oil and coal. Together with the increasing energy demand in the world it is clear that there is a necessity for new environmentally friendly energy sources. This is where fusion comes in.

Thermonuclear fusion is the energy source of the stars. It is the process where two nuclei merge to one nucleus that has a lower binding energy and therefore energy is released. The most promising candidates for fusion energy production involves the hydrogen isotopes deuterium (D) and tritium (T) in the following reactions:

$$\mathrm{D} + \mathrm{D} \longrightarrow \mathrm{He}^3 + n + 3.27 \text{ MeV} \tag{1.1a}$$

$$\mathrm{D} + \mathrm{D} \longrightarrow \mathrm{T} + \mathrm{H} + 4.05 \text{ MeV} \tag{1.1b}$$

$$\mathrm{D} + \mathrm{T} \longrightarrow \mathrm{He}^4 + n + 17.58 \text{ MeV} \tag{1.1c}$$

The reaction probability and energy output is highest for the D-T reaction, with the resulting energy shared by the neutron (80%) and the helium isotope (20%), henceforth referred to as the alpha particle, and will probably dominate future fusion reactors. However, present day experiments are mainly run with D-D reactions that have a significantly lower flux of neutrons.

In order to bring two positive nuclei close enough to fuse the repulsive Coulomb force needs to be overcome. The temperature required to accomplish economically feasible thermonuclear fusion here on Earth is approximately

10^8K, which is higher than the temperature at the center of the Sun. At these temperatures the gas is completely ionised and is known as a *plasma*.

To use nuclear fusion as an energy source the plasma needs to be confined. In stars, confinement of the plasma is provided by gravitation. Here on Earth, magnetic confinement is currently the main scheme for confinement. It uses the basic fact that a plasma consists of charged particles which follow magnetic field lines. The physical problem to solve is the design of the magnetic field topology for confinement.

Tokamaks [2] are axisymmetric, toroidal configurations that confine plasma particles through the use of an externally generated toroidal magnetic field with a smaller poloidal magnetic field generated inside the device by running a current through the plasma. There is a large number of tokamak experimental facilities operating or being constructed, the largest currently in operation is the Joint European Torus (JET). JET holds the world fusion power record of 16 MW from a total input power of 24 MW [3]. The largest experimental tokamak facility, currently under construction, is the internationally funded facility ITER, which will have a plasma volume of 840 m^2 (compared to JET which has 100 m^2). The main objectives of ITER are to momentarily produce ten times more thermal energy from fusion heating than is supplied by auxiliary heating and to maintain a substantially longer discharge (up to eight to ten minutes) than current experiments [4].

1.2 Turbulent Transport

The performance of a fusion facility is measured by the so called *fusion triple product*, $n_i T_i \tau_E$ [5]. Here, n_i and T_i are the density and temperature of ions that together form the thermal pressure $p_i = n_i T_i$, and τ_E is the *energy confinement time*, which is the relaxation time of the plasma due to heat conduction and is tied to the plasma volume. In a tokamak, the pressure is limited by large scale *magnetohydrodynamic* instabilities. Therefore, in order to significantly increase the fusion triple product, the confinement time needs to be increased, which requires a better understanding of transport of particles, heat and momentum in the plasma.

The mimimum level of transport is *classical* transport due to collisions or when the non-uniform magnetic field of a tokamak is taken into account *neoclassical* transport. For both a random walk estimate can be used to calculate heat and particle diffusivities which in turn predict transport through energy and particle conservation equations. Although the neoclassically obtained diffusivities are higher than those obtained from classical transport theory alone, experimental measurements are orders of magnitude higher in most regions of the plasma [6]. This enhanced level of transport, often re-

ferred to as *anomalous*, is caused by small scale, low frequency fluctuations called *microinstabilities* [7]. One important class of microinstabilities are *drift waves*. Gradients in temperature or density may cause an exponential growth of the amplitude of these fluctuations. Nonlinear interactions then saturate the growth of the fluctuation amplitude, generating turbulence and setting a quasi-steady state level of the heat and particle fluxes. There are a multitude of different models, mostly relying on numerical methods, to describe this complex nonlinear behaviour, each with different simplifying assumptions and level of sophistication. From input parameters, which consist of the equilibrium magnetic field together with density and temperature profiles, these transport models predict the ensuing turbulent fluctuations and the associated fluxes. These in turn can be compared to experimentally obtained fluxes, thus validating the model.

1.3 Theoretical Descriptions of Plasmas

There are different basic approaches used to decribe a plasma. The first is *single particle motion theory* where the trajectory of each charged particle is studied in a given electromagnetic field. This is not really a plasma theory, though it gives an intuitive picture of the particle dynamics occuring in the plasma. Naively, to describe the plasma self-consistently would consist of following the trajectories of each particle under the influence of external and internal electromagnetic fields. For n particles ($\sim 10^{19}$ in JET), the result is N ($\sim 10^{21}$ in JET) nonlinear coupled differential equations to be solved simultaneously which is not possible in practice.

Kinetic theory is based on a statistical approach in which the plasma is described in terms of a *distribution function* $f(\vec{x}, \vec{v}, t)$, where $f(\vec{x}, \vec{v}, t)d\vec{x}d\vec{v}$ is the probability of finding particles within the *phase space* element of volume $d\vec{x}d\vec{v}$, centered at $(\vec{x}, \vec{v})$. The problem then consists of solving the kinetic equation system which governs the evolution of the distribution function in phase space. Though kinetic theory, together with Maxwells equations, provides an accurate description of the plasma, further simplifications are useful. One such simplified model is *fluid theory* in which the plasma is described by the interaction of multiple fluids and macroscopic quantities such as densities, temperatures and pressures are used to describe the plasma. These quantities are derived from the velocity space moments of the distribution function for each plasma species. Accordingly, fluid equations describing the conservation of density, momentum, energy and so forth are obtained by the velocity moments of the previously mentioned kinetic equation. When using the moment procedure, it always leads to a system of more unknowns than equations so one needs to truncate the series of moments by some assumtions, usually referred to as clo-

sure. Finally, in *magnetohydrodynamic (MHD) theory*, ion and electron fluids are combined into one single fluid. It is often used to describe the macroscopic fusion plasma behavior such as plasma equilibrium and global instabilities.

1.4 Heating and Fast Ions

Although tokamak plasmas are automatically heated ohmically by the current in the plasma, external heating schemes are also necessary, such as neutral beam injection (NBI) and radio frequency heating. NBI consists of a highly energetic beam of neutrals injected into the plasma where they are ionized and heat the plasma through collisions while radio frequency waves heat the plasma through resonant interaction between circularly polarized waves and the gyrating plasma particles. In a burning fusion D-T plasma, such as in ITER, self-heating by the fusion generated alpha particles will be the most important mechanism to heat and maintain the plasma temperature. Common to all these heating schemes is the resulting highly energetic ions with velocities greatly exceeding the thermal velocity of ions in the plasma. As these fast ions decelerate due to collisions they transfer their energy to the background ions and electrons.

The presence of energetic ions, mainly in the plasma core, affects heating and transport of particles in the plasma through two main mechanisms [8]. First, since these ions are not in thermodynamical equilibrium, the free energy available in their velocity distribution can destabilize wave like perturbations in the equilibrium plasma when the motion of the fast ions matches that of the wave phase velocity. A destabilization of the perturbation occurs when the fast particle pressure is large enough to overcome the total damping by the bulk plasma [9]. One important class of magnetohydrodynamic perturbations is the *shear Alfvén waves*. These waves oscillate at relatively low frequencies and propagate at the characteristic *Alfvén speed*. As the fast ions slow down they can destabilize and interact with various Alfvénic waves (cf. [10]). Fast ions also affect the turbulent transport of the background ions and electrons caused by microinstabilities in the plasma. This in turn affects the confinement time as well as the radial density and temperature profiles. The inclusion of a fast ion species has been shown to have a stabilizing influence on turbulent transport driven by the so called *Ion Temperature Gradient mode* [11–13] which is commonly believed to be the dominant drift wave instability limiting confinement in a tokamak plasma. The stabilizing effects are due to the increased total thermal pressure and pressure gradient by the presence of fast ions [11, 14, 15] and a dilution effect of the main ions that drive the instability [16].

The remainder of this thesis is organized as follows: In Chapter 2, we in-

troduce the concept of waves as oscillating perturbations in electric and magnetic fields in the plasma. We present the toroidal Alfvén eigenmode (TAE), which exists due to the toroidal geometry of a tokamak. Then, in Chapter 3, a heuristic one-dimensional electrostatic "bump-on-tail" model is used to describe nonlinear aspects of wave-particle interaction, where the instabilities are driven by a low density population of highly energetic electrons at the tail of the bulk electron distribution function. We finish Chapter 3 with a brief discussion on the connection between the one-dimensional model and the three dimensional tokamak geometry. Chapter 4 is devoted to turbulent particle transport and the resulting peaking of the density profile. Two theoretical transport models, used to analyze drift wave turbulence, are presented as well as a transport code where the plasma profiles are simulated and compared to the experimentally obtained profiles. Finally, Chapter 5 consists of a brief summary of the appended papers.

2

Toroidal Systems

Magnetic confinement of plasma particles can be implemented in several different ways. Many of these methods utilize externally generated magnetic fields designed in such a way that the field lines define a torus, i.e a cylinder deformed until it closes on itself. The most common type of toroidal magnetic confinement device is the *tokamak*. In tokamaks, the plasma particles are mainly confined by means of a large magnetic field in the toroidal direction, which is generated by external coils. This results in circulating particles that follow the magnetic field lines around the torus. However, a small poloidal field component produced by a transformer induced plasma current is also necessary in order to average out radial drifts. This is because the toroidal magnetic field varies radially in space, with associated so called ∇B- and curvature drifts of the particles resulting in a vertical separation of electrons and ions. The charge separation leads in turn to a potential difference and an associated $\vec{E} \times \vec{B}$- drift, which results in a radial drift outwards of both ions and electrons.

In general, a tokamak cross section may be elliptically elongated, D-shaped and asymmetric with respect to the horizontal and vertical midplanes. In this thesis, a circular approximation described by the toroidal coordinates (r, θ, ζ) will be used. Here r is the radius, θ is the poloidal angle (short way around) and ζ is the toroidal angle (long way around).

In this chapter we start by introducing the Magnetohydrodynamic model in Sec. 2.1 that is often used to analyze plasma equilibria and linear perturbations with low oscillation frequency. Then, in Sec. 2.2, we study single charged particle motion in the presence of an electromagnetic field in the toroidal geometry. Finally, in Sec. 2.3, we consider Alvénic waves in cylindrical and toroidal geometry. We discuss the possible destabilization of these waves due to interaction with energetic particles.

2.1 Magnetohydrodynamic Model

In MHD, ion and electron fluids are combined into one single fluid. For the MHD description to be valid the plasma needs to be collision dominated, i.e locally Maxwellian, which means that the considered time scale must be sufficiently long for there to be adequately many collisions. The displacement current can then be neglected in Maxwell's equations. This means that the time scale is much longer than the time it takes light to traverse the plasma. Furthermore, the dominant fluid velocity is the $\vec{E} \times \vec{B}$-drift, which means that MHD describes low frequency phenomena.

The characteristic properties of the MHD fluid are expressed by

- the total mass density
$$\rho \equiv m_i n_i + m_e n_e \ , \tag{2.1}$$
- the total charge density
$$\rho_c \equiv e(Z_i n_i - n_e) \ , \tag{2.2}$$
- the center-of-mass velocity
$$\vec{v} \equiv \frac{m_i n_i \vec{v}_i + m_e n_e \vec{v}_e}{m_i n_i + m_e n_e} \approx \vec{v}_i \ , \tag{2.3}$$
- the current density
$$\vec{J} \equiv e(Z_i n_i \vec{v}_i - n_e \vec{v}_e) \ , \tag{2.4}$$
- and the total scalar pressure
$$P = P_e + P_i \ , \tag{2.5}$$

where $m_i, m_e, n_i, n_e, \vec{v}_i, \ \vec{v}_e, \ P_i$ and P_e are the masses, number densities, fluid velocities and pressure of ions and electrons, respectively, Z_i is the ion charge number and e is the magnitude of the electron charge. With the assumption of quasi-neutrality, $Z_i n_i \approx n_e$, one finds $\rho_c = 0$ and the MHD set of equations are

- the continuity equation
$$\frac{\partial \rho}{\partial t} + \nabla \cdot (\rho \vec{v}) = 0 \ , \tag{2.6a}$$
- the momentum equation
$$\rho \frac{d\vec{v}}{dt} = \vec{J} \times \vec{B} - \nabla P \ , \tag{2.6b}$$

- the adiabatic equation of state

$$\frac{d}{dt}\left(\frac{P}{\rho^{\gamma}}\right) = 0 \ , \tag{2.6c}$$

- the resistive Ohm's law

$$\vec{E} + \vec{v} \times \vec{B} = \eta \vec{J} \ , \tag{2.6d}$$

- Ampére's law (without the displacement current)

$$\nabla \times \vec{B} = \mu_0 \vec{J} \ , \tag{2.6e}$$

- and Faraday's law

$$\nabla \times \vec{E} = -\frac{\partial \vec{B}}{\partial t} \ . \tag{2.6f}$$

Here, γ is the ratio of specific heats at constant pressure and constant volume, η is the plasma resistivity and μ_0 is the permeability of free space. Note that the Maxwell relation $\nabla \cdot \vec{B} = 0$ is implied. The fact that the displacement current is neglected in Ampére's law also means that

$$\nabla \cdot \vec{J} = 0 \ . \tag{2.7}$$

In many cases a further simplification is made by assuming that the plasma conductivity is high enough that the right hand side of Ohm's law can be neglected. The resulting model is called ideal MHD and one of its consequences is that the parallel component of the electric field is zero. It is not obvious that the criteria for ideal MHD are fulfilled. However, it seems to provide an accurate description of the macroscopic fusion plasma behavior [17] and is thus frequently used to describe plasma equilibrium and stability of waves. For that reason we will use it for the basic analysis of low frequency Alfvén waves in this thesis.

2.1.1 Equilibrium Analysis

Tokamak magnetic equilibria can be calculated using the ideal MHD force balance equation

$$\vec{J} \times \vec{B} = \nabla P \ , \tag{2.8}$$

where $\vec{J}$ is the plasma current and p the total particle pressure. The resulting *flux surfaces*, corresponding to surfaces of constant pressure, close on themselves both toroidally and poloidally, and must therefore be nested tubes with the innermost being the magnetic axis. Hence, $P = P(\psi)$, where ψ, the

poloidal flux (or toroidal flux), is constant along magnetic field lines, i.e a function only of r. The poloidal and toroidal magnetic flux can be expressed as

$$\psi_P = \frac{1}{2\pi}\int_{V(r)} \vec{B}\cdot\nabla\theta \,\mathrm{d}^3x \ , \tag{2.9a}$$

$$\psi_t = \frac{1}{2\pi}\int_{V(r)} \vec{B}\cdot\nabla\zeta \,\mathrm{d}^3x \ , \tag{2.9b}$$

where $\mathrm{d}^3x = J^{-1}\mathrm{d}r\mathrm{d}\theta\mathrm{d}\zeta$, J is the Jacobian and $V(r)$ is the volume bounded by the magnetic flux surface of radius r. They are related by the safety factor

$$q = \frac{\vec{B}\cdot\nabla\zeta}{\vec{B}\cdot\nabla\theta} \ , \tag{2.10}$$

which is equal to the number of toroidal revolutions a field line executes during one poloidal revolution.

In a tokamak, we may express the magnetic field with a toroidal and a poloidal component $\vec{B} = \vec{B}_T + \vec{B}_P$, where $B_T \gg B_P$ and the toroidal magnetic field strength varies radially as R^{-1}:

$$B_T \propto \frac{1}{R} = \frac{1}{R_0(1+\epsilon\cos\theta)} \ . \tag{2.11}$$

Here, R_0 is the distance from the axis of symmetry to the magnetic axis and

$$\epsilon \equiv r/R_0 \ , \tag{2.12}$$

is the inverse aspect ratio, which is generally small throughout a tokamak.

2.1.2 Linear Stability Analysis

When we have an equilibrium plasma the next step is to look at its stability properties. To simplify the analysis we will restrict ourselves to linear stability, and represent the dependent variables as the sum of an equilibrium part plus a small perturbation,

$$\vec{B} = \vec{B}_0 + \vec{B}_1 \ , \quad \vec{J} = \vec{J}_0 + \vec{J}_1 \ , \tag{2.13a}$$

$$P = P_0 + P_1 \ , \quad \rho = \rho_0 + \rho_1 \ , \tag{2.13b}$$

where the equilibrium and perturbed quantities are denoted by the subscripts 0 and 1, respectively. We can transform the MHD equations to a frame of reference moving with the equilibrium velocity $\vec{v}_0$, which means that $\vec{v} = \vec{v}_1$ and, by ideal Ohm's law, $\vec{E} = \vec{E}_1$. The equilibrium quantities are then functions of space only while the perturbations are of space and time. From the set of

equations (2.6a) - (2.6f), with ideal Ohm's law, we obtain sets of equations to zeroth order for the equilibrium (2.8) and to first order for the stability:

$$\frac{\partial \rho_1}{\partial t} + \nabla \cdot (\rho_0 \vec{v}_1) = 0 \ , \tag{2.14a}$$

$$\rho_0 \frac{\partial \vec{v}_1}{\partial t} = \vec{J}_0 \times \vec{B}_1 + \vec{J}_1 \times \vec{B}_0 - \nabla P_1 \ , \tag{2.14b}$$

$$\frac{\partial P_1}{\partial t} + \vec{v}_1 \cdot \nabla P_0 + \frac{\gamma P_0}{\rho_0} \left(\frac{\partial \rho_1}{\partial t} + \vec{v}_1 \cdot \nabla \rho_0 \right) = 0 \ , \tag{2.14c}$$

$$\frac{\partial \vec{B}_1}{\partial t} = \nabla \times (\vec{v}_1 \times \vec{B}_0) \ , \tag{2.14d}$$

$$\nabla \times \vec{B}_1 = \mu_0 \vec{J}_1 \ . \tag{2.14e}$$

The resulting eigenvalue problem needs to be solved for a given magnetic field in a certain geometry, with given initial values and boundary conditions. The simplest case of a homogeneous magnetic field in an infinite geometry results in two kinds of waves, the shear and compressional Alfvén waves. For us the most interesting is the shear Alfvén wave

$$\omega^2 = k_\parallel^2 v_A^2 \ , \tag{2.15}$$

where $k_\parallel$ is the parallel wave number with respect to the background magnetic field and v_A is the Alfvén speed

$$v_A^2 \equiv \frac{B_0^2}{\mu_0 \rho_0} \ . \tag{2.16}$$

This wave propagates along and at angles to the magnetic background field but the fluctuation in the magnetic field is perpendicular to it (i.e $\vec{B}_1 \perp \vec{B}_0$), hence the name shear wave. Furthermore, this wave has no density or pressure fluctuations (i.e $P_1 = \rho_1 = 0$) and is therefore said to be incompressible.

2.2 Single Particle Motion

The motion of a charged particle in the presence of a given electromagnetic field consists of a rapid gyration around the so called *guiding center position*, motion along the field line (with a possible acceleration/deceleration) and a drift across it. The gyrating motion is known as *Larmor gyration* and the frequency is the *cyclotron frequency*, $\omega_c = ZeB/m$.

In the absence of wave fields, the trajectory of a particle can be characterized by the following three invariants of motion: First, the total particle energy

$$E = W + Ze\phi \tag{2.17}$$

consists of a sum of the kinetic- $W = mv^2/2$ and potential energy. Second, the generalized toroidal momentum

$$p_\zeta = mR^2 \frac{d\zeta}{dt} - Ze\psi \ , \tag{2.18}$$

where $\psi = 2\pi\psi_P$ is the normalized poloidal flux. Note that in the presence of an external wave field the axisymmetry will be broken and p_ζ and E are no longer constants of motion. However, it can be shown that, when the wave evolves slowly,

$$\dot{p_\zeta} - \frac{n}{\omega}\dot{E} = 0 \ , \tag{2.19}$$

holds. Here, n and ω are the poloidal mode number and wave frequency, defined in Sec. 2.3. This is simply a consequence of the dependence of the perturbed wave field on ζ and t, which only enters as the combination $\omega t - n\zeta$ in the exponential of Eq. (2.21) when we are dealing with isolated modes with a single n. Finally, due to the periodicity of the particles gyration around a magnetic field line, it can be shown that the magnetic moment

$$\mu = \frac{mv_L^2}{2B} \ , \tag{2.20}$$

is an adiabatic invariant, i.e constant as long as the gradients in the magnetic field are sufficiently small as compared to the plasma dimensions and the time scale of variation is long compared to the gyration frequency. This is true in a tokamak since the magnetic field varies on a large scale as compared to the radius of gyration, the *Larmor radius*, r_L. Here, $v_L = r_L\omega_c$ is the constant angular velocity of the gyrating particle.

Trapped and Passing Particles

Since the magnetic field strength in a tokamak falls of with the distance from the axis of symmetry (2.11), particles on the outboard side of the tokamak will experience an increasing magnetic field as they follow the field line. Due to the conservation of the magnetic moment μ, this means that the perpendicular velocity of the particle increases as well which in turn reduces the parallel velocity. Hence, there are two kinds of particles, trapped and passing particles. The trapped particles bounce toroidally and poloidally at the points where their velocities parallel to the total magnetic field vanish, while the passing particles encircle the magnetic axis and the torus toroidally and poloidally. Due to the curvature and ∇B-drifts, the particle orbits may also differ slightly radially from the magnetic flux surfaces. This is known as finite Larmor radius effects (FLR).

2.3 Toroidal Instabilities

In periodic, toroidal systems, any linear quantity may be Fourier decomposed according to

$$\phi(r,\theta,\zeta;t) = \sum_{m,n} \phi_{m,n}(r) e^{i(n\zeta - m\theta - \omega t)} \ , \tag{2.21}$$

where m and n are the so called poloidal and toroidal mode numbers. If the inverse aspect ratio ϵ is small, as in tokamaks, the equilibrium magnetic field is dominated by the toroidal magnetic field (2.11). This magnetic field is symmetric in ζ, but because of the poloidal variation there is no symmetry in θ. For Alfvén type instabilities this leads to a coupling between neighboring poloidal harmonics of ϕ. If we assume that the mode numbers m and n are large, the equations describing this coupling are [18]

$$\begin{bmatrix} \mathfrak{L}_m & \mathfrak{L}_1 \\ \mathfrak{L}_1 & \mathfrak{L}_{m-1} \end{bmatrix} \begin{bmatrix} \phi_m \\ \phi_{m-1} \end{bmatrix} = 0 \ , \tag{2.22}$$

where

$$\mathfrak{L}_m = \frac{d}{dr}\left[\left(\frac{\omega^2}{v_A^2} - k_{\parallel m}^2\right)\frac{d}{dr}\right] - \frac{m^2}{r^2}\left(\frac{\omega^2}{v_A^2} - k_{\parallel m}^2\right) \ , \tag{2.23a}$$

$$\mathfrak{L}_1 = \frac{\hat{\epsilon}}{4q^2R_0^2}\frac{d^2}{dr^2} \ . \tag{2.23b}$$

Here $k_{\parallel m}$ is the parallel wave number with respect to the magnetic field given by

$$k_{\parallel m} \equiv \vec{k}\cdot\vec{B}_0/B_0 = \frac{nq(r)-m}{q(r)R_0} \ , \tag{2.24}$$

v_A is the Alfvén speed (2.16), q is the safety factor (2.10) and in [19] it was shown that $\hat{\epsilon} \approx 5r/2R_0$. Note that the toroidal mode number n is suppressed in Eqs. (2.22)-(2.24) since it holds for any large enough n.

2.3.1 Cylindrical Limit

In the cylindrical limit $\epsilon \to 0$, the magnetic field strength is constant. This means that the translational symmetry in θ is restored, and the set of coupled equations (2.22) decouples into an equation for each poloidal harmonic satisfying

$$\frac{d}{dr}\left[\left(\frac{\omega^2}{v_A^2} - k_{\parallel m}^2\right)\frac{d\phi_m}{dr}\right] - \frac{m^2}{r^2}\left(\frac{\omega^2}{v_A^2} - k_{\parallel m}^2\right)\phi_m = 0 \ , \tag{2.25}$$

for each poloidal harmonic. A particularly easily found branch of solutions to (2.25) has $\omega^2 = \omega_A^2 = k_{\parallel m}^2 v_A^2$. According to Eq. (2.25), however, such

modes have logaritmically divergent mode amplitudes and furthermore are almost completely damped due to the radial dispersion (well defined radial wave packages simply deconstruct since their constituents travel at different phase velocities, a process known as phase mixing) [20]. This damping is known as *continuum damping* and the radial spectrum of the logaritmically divergent modes is called *Alfvén continuum*, whose qualitative behavior is plotted in Fig. (2.1).

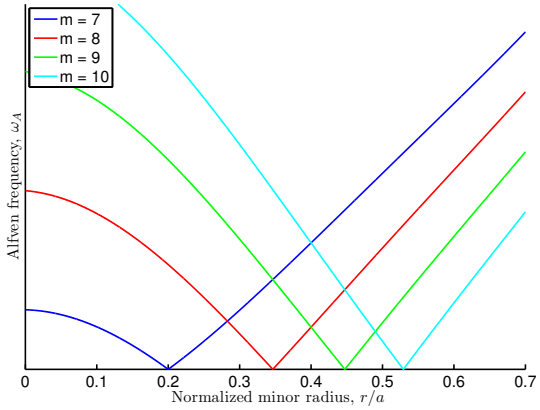

Figure 2.1: Qualitative figure displaying the Alfvén frequency ω_A, decreasing along the branch $-k_{\parallel\, m\, n}(r)v_A(r)$ from $r = 0$ until $k_{\parallel\, m\, n} = 0$ and then increase monotonically along $k_{\parallel\, m\, n}(r)v_A(r)$ to the plasma edge, when $n = 5$ and m ranges from 7 to 10.

2.3.2 Toroidal Alfvén Eigenmodes

Toroidal Alfvén eigenmodes (TAEs) are discrete frequency waves [21] that exist due to toroidicity induced coupling between poloidal harmonics. In the cylindrical limit, neighbouring poloidal continua cross at the surfaces $r = r_m$ (see Fig. 2.1), where for a given n

$$k_{\parallel\, m} v_A = -k_{\parallel\, m+1} v_A \equiv \omega_0 \ , \tag{2.26}$$

which implies that

$$q\left(r_m\right) \equiv q_m = \frac{2m+1}{2n} \ . \tag{2.27}$$

Inserting (2.27) in (2.26) yields

$$\omega_0 = \frac{v_A}{2q_m R_0} \ . \tag{2.28}$$

Accounting for toroidicity by letting ϵ become finite, only affects the proximity of r_m, where small gaps of width $\Delta\omega \approx \hat{\epsilon}\,\omega_0$ are induced in the Alfvén continuum, see Fig. 2.2. The distance between such neighboring gaps is approximately [22]

$$|r_{m+1} - r_m| \approx \frac{r_m}{nqs} \ , \tag{2.29}$$

where the magnetic shear s is defined as

$$s \equiv \frac{r}{q}\frac{dq}{dr} \ . \tag{2.30}$$

Nonzero ϵ also results in a discrete frequency eigenmode, which forms due to

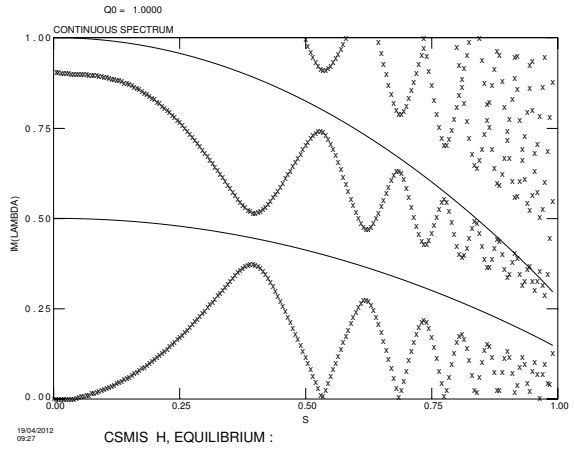

Figure 2.2: Alfvén continuum for $n = 4$, discharge #42979 at JET. The equilibrium was reproduced with the MHD equilibrium code HELENA [23] and the continuum by the MHD linear instability code CSCAS. Here, radial variable is $s \propto \sqrt{\psi}$ and $Im[\lambda] \propto \omega_A$.

the interaction of neighboring poloidal harmonics in the vicinity of the gap. In the low shear limit, $s \ll 1$, the distance between the gaps is sufficiently large for the eigenmode to be localized near its own gap and not interact with modes from neighboring gaps. According to boundary layer theory [22] the coupling between different harmonics takes place in a narrow inner region and in the outer region each poloidal mode satisfies a cylindrical mode equation. To determine the mode structure, a matching procedure for the outer and inner regions has to be used [22]. The result in the low shear limit is a discrete frequency eigenmode at the bottom of each toroidicity induced gap with the frequency given by

$$\omega_{TAE} = \omega_0 \left[1 - \hat{\epsilon}\left(1 - \frac{\pi^2 s^2}{8}\right)\right] \ . \tag{2.31}$$

Since the mode is inside the gap it does not fulfill the condition for continuum damping. This eigenmode is therefore weakly damped and it consists of an even combination of the coupled neighboring poloidal harmonics, see Fig. 2.3.

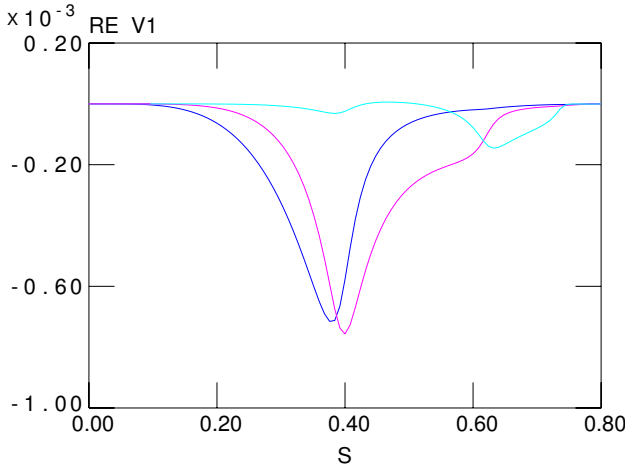

Figure 2.3: Radial structure for coupled, neighbouring poloidal harmonics constituting an even TAE for $n = 4$, discharge #42979 at JET with corresponding continuum in Fig. 2.2. The mode is localized around the first radial gap, but the tail of one of the poloidal harmonics reaches into the next gap. The eigenmode is found by means of the spectral MHD code MISHKA [24].

Note that the theory presented here only gives criteria for the existance of toroidal Alfvén eigenmodes. A driving mechanism is needed to excite these modes, such as e.g. resonant interaction between the wave and fast particles.

2.3.3 Energetic Particle Drive

The TAE modes described in the previous section have been derived within the framework of ideal MHD, using a linear approach where all quantities are assumed to consist of a stationary part and a small perturbation. This results in a real frequency $\omega = \omega_{TAE}$. Fast ions on the other hand, with $v_f \gg v_{th}$, where v_{th} is the thermal velocity of the bulk ions in the plasma, need to be treated using kinetic theory. The result can then be added to the MHD result, with the fast particles contributing to the imaginary part of the linear frequency, which becomes $\omega = \omega_{TAE} + i\gamma_L$ [25]. Since all perturbed quantities vary in time as $e^{-i\omega t}$, the fast particles result in an exponential growth of the wave provided that $\gamma_L > 0$. This also means that the linear theory is only valid initially. Free energy is available to drive the mode when the fast particle pressure is large enough to overcome the total damping by the bulk plasma [26, 27]

3

Wave-Particle Interaction

This chapter is dedicated to the study of single, isolates modes in the presence of energetic particles. By means of action-angle variables and the framework of canonical transformations, particle motion in a single TAE mode with reasonably well defined frequency can be described by a one-dimensional model [28]. This can be conceptually understood since even in the presence of a an external wave field the particle motion is characterized by two constants of motion, as described in Sec. 2.2.

In this chapter we start by considering electrostatic longitudinal waves in a one-dimensional uniform plasma. In Sec. 3.1 the plasma is considered cold and a fluid description is used to describe the mode oscillations. Then, in Sec. 3.2, thermal effects are included. Kinetic theory is then employed to investigate the effect of finite plasma particle velocities, and we will see that this leads to substantial interaction between a group of particles travelling at roughly the *phase velocity* of the wave and the wave itself. Those particles are called resonant, and their interaction with the wave leads to exponential damping (or growth) of the wave amplitude, known as Landau damping/drive, that is phenomenonically described in Sec. 3.3. In Sec. 3.4 we study the nonlinear wave-particle interaction using a simple one-dimensional electrostatic "bump-on-tail" model, in which the resonance lies in the high energy tail of the distribution from the bulk electrons and a bunch of extra electrons have been added around the resonance to mimic fast particles in a tokamak. Finally, in Sec. 3.5, we make a connection between the one-dimensional model and the three-dimensional geometry of a tokamak.

3.1 Electrostatic Plasma Waves in a Cold Plasma

We consider an electrostatic wave with spatial period λ and wave number $k = 2\pi/\lambda$ in a one-dimensional uniform, static plasma fulfilling $v_{th} \ll \omega/k$, where v_{th} is the thermal velocity of the electrons and ω is the wave carrier frequency. The wave can be treated as a small perturbation to the stationary and homogeneous background plasma, which in this limit is considered cold. The wave frequency is high enough that the ions are unaffected by the wave field due to their much larger mass, and therefore do not contribute to the dynamics except to keep the equilibrium plasma neutral, $n_i = n_{i0}$. The electron density and velocity on the other hand are decomposed as an unperturbed part and a small perturbation, $n_e = n_{e0} + \delta n_e$ and $v_e = v_{e0} + \delta v_e$, where $n_{e0} = n_{i0}$ and we set $v_{e0} = 0$. As always in connection with the latter assumption, we consider the case when the electric field, $E(x;t)$, is purely a wave quantity and thus has no equilibrium part either, so that there is no net acceleration of the plasma as a whole. We assume that the electric field is small enough that fluid nonlinearities are unimportant. The electrons then respond linearly to the electric field and their perturbed velocity and perturbed density satisfies the linearized fluid equation of motion and the continuity equation

$$\frac{\partial \delta v_e}{\partial t} = -\frac{e}{m_e} E \ , \tag{3.1a}$$

$$\frac{\partial \delta n_e}{\partial t} + n_{e0} \frac{\partial \delta v_e}{\partial x} = 0 \ , \tag{3.1b}$$

where e and m_e are the (magnitude of the) charge and mass of the electron, respectively. Now, the Poisson equation provides closure,

$$\frac{\partial E}{\partial x} = \frac{e}{\epsilon_0}(n_i - n_e) = -\frac{e}{\epsilon_0}\delta n_e \ , \tag{3.2}$$

where ϵ_0 is the permittivity of free space. We express the electric field using the electrostatic potential $E = -\partial \Phi/\partial x$, and since the equations are linear we Fourier expand the perturbed quantities,

$$\Phi, \delta v_e, \delta n_e \sim e^{i(kx - \omega t)} \ . \tag{3.3}$$

The differential equations (3.1) - (3.2) then become algebraic and can be combined to give the *dispersion relation*

$$\omega^2 = \omega_{pe}^2 \equiv \frac{e^2 n_{e0}}{\epsilon_0 m_e} \ . \tag{3.4}$$

i.e a function on the form $\omega = \omega(k)$. This wave is called the longitudinal wave since it propagates parallel to the electric field. The lack of an oscillating magnetic field makes this a purely electrostatic wave. Also, there is no depencence

on k in the dispersion relation, which means that there is no dispersive effect. This is the reason that we will later choose this particular mode to emulate a TAE mode in Section 3.4.

3.2 Warm Plasma Waves: Linear Landau Damping

The effect of thermal plasma particle motion on the system described in the previous section is obtained by the inclusion of a nonzero electron pressure term in (3.1a) and an equation of state relating the electron pressure and density. The dispersion relation (3.4) gets a small thermal correction which introduces dispersion of the wave by the inclusion of a k-dependent term, but the method misses the important hot-plasma contribution from particles energetic enough to interact resonantly with the wave field. In order to describe wave-particle interaction kinetic theory is used. We limit ourselves to a uniform plasma described in terms of a distribution function $f(x, v, t)$ that evolves in phase space according to the *Vlasov equation*

$$\frac{\partial f}{\partial t} + \dot{x}\frac{\partial f}{\partial x} + \dot{v}\frac{\partial f}{\partial v} = 0 \ , \tag{3.5}$$

where $\dot{v} = -eE/m_e$ and collisions have been neglected. We consider a perturbative solution by expansion of the distribution function according to

$$f = F_0 + \delta f \ . \tag{3.6}$$

Here, F_0 is the equilibrium, or *unperturbed*, distribution function in the absence of wave fields. It is static by definition, $\partial F_0/\partial t = 0$. Also, the uniform equilibrium plasma fulfills $\partial F_0/\partial x = 0$ which means that $F_0 = F_0(v)$. The term $\delta f \ll F_0$, is a perturbation from the equilibrium distribution due to the wave field. To linear order, the Vlasov equation (3.5) becomes,

$$\frac{\partial \delta f}{\partial t} + v\frac{\partial \delta f}{\partial x} - \frac{eE}{m_e}\frac{dF_0}{dv} = 0 \ . \tag{3.7}$$

We Fourier expand the perturbed quantities,

$$E, \delta f \sim e^{i(kx-\omega t)} \ , \tag{3.8}$$

and Eq. (3.7) becomes an algebraic expression for the perturbed distribution function

$$\delta f = i\frac{eE}{m_e}\frac{dF_0/dv}{\omega - kv} \ . \tag{3.9}$$

The Poisson equation provides closure,

$$\frac{\partial E}{\partial x} = -\frac{e}{\epsilon_0}\delta n_e = -\frac{e}{\epsilon_0}\int \delta f \, dv \ , \tag{3.10}$$

which by Fourier expansion, together with (3.9) results in a dispersion relation on the form,

$$1 + \frac{\omega_{pe}^2}{k}\int \frac{d\hat{F}_0/dv}{\omega - kv}\, dv = 0 \ . \tag{3.11}$$

Here, $\hat{F}_0$ is normalized with n_{e0} so that $\int \hat{F}_0(v)\, dv = 1$. Note that the integral in Eq. (3.11) diverges at $v = \omega/k$. This means that the particles with velocities close to this *resonant velocity* will interact heavily with the wave. Landau was the first to properly treat this integral [29]. For the weakly damped wave with frequency ($\omega >> kv_{th}$) we calculate an approximate solution when $\hat{F}_0$ is taken to be a Maxwellian distribution function,

$$\hat{F}_0 = \frac{1}{\sqrt{\pi} v_{th}} e^{-v^2/v_{th}^2} \ , \tag{3.12}$$

where the thermal velocity v_{th} is defined using

$$\frac{m_e v_{th}^2}{2} \equiv k_B T \ , \tag{3.13}$$

and k_B is Boltzmanns constant. In the weakly damped case $\mathrm{Im}[\omega]$ is small and the integration contour is a straight line along the $\mathrm{Re}[v]$ axis with a small semicircle *under the pole* at $v = \omega/k$. Eq. (3.11) becomes (cf. [30])

$$1 - \frac{\omega_{pe}^2}{k^2}\left[P\int_{-\infty}^{\infty} \frac{d\hat{F}_0/dv}{v - \omega/k}\, dv + i\pi \left.\frac{d\hat{F}_0}{dv}\right|_{v=\frac{\omega}{k}} \right] = 0 \ , \tag{3.14}$$

where the first term inside the bracket is the *Cauchy principal value* of the integral and the second is $i\pi$ times the *residue* at the pole, corresponding to the contribution from the nonresonant particles and the resonant particles, respectively. For the nonresonant particles, $d\hat{F}_0/dv$ is negligably small for large enough velocities, say nv_{th} ($n > 1$), which allows us to limit the evaluation of the integral to this velocity. In this limit we Taylor expand,

$$\frac{1}{v - \omega/k} \simeq -\frac{k}{\omega}\left[1 - \frac{kv}{\omega} - \left(\frac{kv}{\omega}\right)^2 - \left(\frac{kv}{\omega}\right)^3 \right] \ . \tag{3.15}$$

and the integral in (3.14) now consists of four terms

$$P\int_{-\infty}^{\infty} \frac{d\hat{F}_0/dv}{v - \omega/k}\, dv \approx \frac{2}{\sqrt{\pi} v_{th}^3}\int_{-\infty}^{nv_{th}} \frac{kv}{\omega}\left[1 - \frac{kv}{\omega} - \left(\frac{kv}{\omega}\right)^2 - \left(\frac{kv}{\omega}\right)^3 \right] e^{-v^2/v_{th}^2}\, dv \ , \tag{3.16}$$

Now, we expand the integration limit to infinity, since any errors this might bring in the Taylor expansion are suppressed by the exponential. In this high frequency limit the first and third terms goes to zero and by calculation of the integral from the second and fourth term we obtain an expression for (3.14) on the form

$$D(\omega) = 1 - \frac{\omega_{pe}^2}{\omega^2} - \frac{3k^2 v_{th}^2}{2}\frac{\omega_{pe}^2}{\omega^4} - i\pi\frac{\omega_{pe}^2}{k^2}\left.\frac{d\hat{F}_0}{dv}\right|_{v=\frac{\omega}{k}} = 0 \ . \tag{3.17}$$

We proceed to find a solution by setting

$$\omega = \omega_R + i\omega_I \ , \tag{3.18}$$

thus,

$$D(\omega) = D_R(\omega_R + i\omega_I) + iD_I(\omega_R + i\omega_I) = 0 \ , \tag{3.19}$$

which we Taylor expand around ω_R assuming a weak damping, i.e. $\omega_I \ll \omega_R$. The resulting dispersion relation becomes [31]

$$\omega = \omega_{pe} + \frac{3v_{th}^2}{4}k^2 + i\gamma_L \ , \tag{3.20}$$

where

$$\gamma_L \equiv \frac{\pi\omega_{pe}^3}{2n_{e0}k^2}\left.\frac{dF_0}{dv}\right|_{v=\frac{\omega}{k}} \ . \tag{3.21}$$

Since the equilibrium distribution function F_0 is taken as a Maxwellian, the slope of the distribution function at the *phase velocity* of the wave $v_{ph} = \omega/k$ is negative which results in a negative γ_L and the wave amplitude experiences damping from the interaction with the resonant particles. This phenomenon is called *Landau damping* and it is not found within the fluid description of the plasma.

3.3 Nonlinear Landau Damping

An intuitive understanding of Landau damping can be gained by studying the motion of single particles in a given electric field

$$E = A\cos(kx - \omega_{pe}t) \ . \tag{3.22}$$

We make a change of variables to a frame that moves at the wave phase velocity

$$kz = kx - \omega_{pe}t - \frac{\pi}{2} \ , \tag{3.23}$$

and the total energy of a particle in this frame of reference is

$$W = \frac{m_e}{2}u^2 + \frac{eA}{k}\cos(kz) \ , \tag{3.24}$$

where $u \equiv v - \omega_{pe}/k$, is the wave-frame velocity. Note that W is essentially the wave frame Hamiltonian, and is therefore a conserved quantity of the particle motion when the electric field amplitude A does not change. We set

$$\omega_A \equiv \sqrt{\frac{eAk}{m_e}} \ , \tag{3.25}$$

which corresponds to a normalization of the mode amplitude that has the dimension of frequency, and invert Eq. (3.24) to give an expression for the particle velocity as function of z, given a value of W,

$$u(z;W) = \pm\sqrt{2\left(\frac{W}{m_e} - \frac{\omega_A^2}{k^2}\cos(kz)\right)} \ . \tag{3.26}$$

In Fig. 3.1 the trajectories of energy W are visualized in phase space. The gray trajectories with $u > 0$ are called co-passing and describe flows in the direction of increasing z, while those with $u < 0$ are called counter-passing and describe flows in the direction of decreasing z. The particles inside the so called *separatrix* (the red curve) are trapped. The trapped particles bounce back and forth with a bounce period given by

$$\tau_B = \int_{z_2}^{z_2}\frac{dz}{u} = \int_{z_1}^{z_2}\left[2\left(\frac{W}{m_e} - \frac{\omega_A^2}{k^2}\cos(kz)\right)\right]^{-1/2} dz \ , \tag{3.27}$$

where z_1 and z_2 are the turning points at which the total energy of the particle matches the electrostatic potential energy, i.e. $u(z_{1,2};W) = 0$. By performing the integration in (3.27) we get

$$\tau_B = \frac{4}{\omega_A}K(\kappa) \ . \tag{3.28}$$

Here, $K(\kappa)$ is the complete elliptical integral of the first kind and we have defined a trapping parameter

$$\kappa^2 \equiv \frac{1}{2}\left(\frac{kW}{eA} + 1\right) < 1 \ . \tag{3.29}$$

The bounce frequency for the trapped particles is then given by

$$\omega_B(W) = \frac{2\pi}{\tau_B} = \frac{\pi\omega_A}{2K(\kappa(W))} \ . \tag{3.30}$$

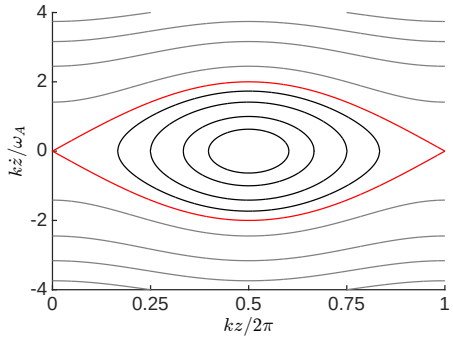

Figure 3.1: *Phase space trajectories of particles in the presence of a sinusoidal electric field* (3.22)*. The wave frame velocity* (3.26) *is normalized in units of* ω_A/k *as defined in Eq.* (3.25)*. The separatrix is highlighted in red.*

The energy dependence of ω_B is the basic mechanism behind Landau damping. It means that trapped particles on different orbits complete their periodic motion at different rates. Particles on deeply trapped trajectories have $\omega_B \sim \omega_A$, but the ones further out have lower rates that tends to 0 at the separatrix orbit. Over time, this variation leads to a phenomenon called *phase mixing* (cf. continuum damping for Alfvén eigenmodes in Sec. 2.3): The skewed orbital frequency profiles effectively averages the particle distribution along the trajectories until it becomes entirely flat throughout the eye-shaped trapped particle area (the region of phase space inside the separatrix). Furthermore, redistribution of particles changes their kinetic energy, so in order for the total energy to remain constant there must be a corresponding energy exchange between the particles and the wave, which means that the wave amplitude ω_A must evolve as a result of the flattening. Consider the case when $dF_0/dv < 0$ at the resonant velocity $v = \omega_{pe}/k$ at $t = 0$, as it is e.g. for the Maxwellian distribution function. Initially, there are more trapped particles in the lower half of the phase space plot in Fig. 3.1 i.e. with velocities just below the phase velocity. So as the phase mixing flattens out the distribution inside the separatrix there is a net transport of particles to higher velocities. That is, a flux of energy from the wave to the particles, which results in a decrease of the wave amplitude referred to as nonlinear Landau damping. Linear Landau damping is recovered within this picture if the perturbation of the distribution function is small enough that the linearized model equation (3.7) remains valid, i.e if the wave is extinguished before the particles complete a full orbit.

Nonlinear effects also dominate if the flux of energy is from the particles to the wave (i.e when $dF_0/dv > 0$ at $v = \omega_{pe}/k$ at $t = 0$) resulting in a drive instead of a damping. Nonlinear analysis in the case of Landau drive will be the subject of Sec. 3.4, however, for now it suffices to say that the mode amplitude

will saturate due to phase mixing and, in principle, an energy balance analysis can be carried out to determine a saturation level of the mode amplitude.

3.4 Bump-on-Tail Model

A low density population of highly energetic electrons is now added to the main or *bulk* plasma. The result is a small "bump" on the tail of the distribution function for the bulk plasma, cf. Fig. 3.2. We are still considering a one dimensional electrostatic plasma wave with a prescribed wavelength λ and wave number $k = 2\pi/\lambda$ in a uniform plasma equilibrium. The wave carrier frequency is assumed to be high enough that the plasma can be separated as a cold bulk whose response can be described using fluid theory while the energetic electrons, which may interact resonantly with the wave, must be treated separately. We include a linear friction force with a damping rate γ_d, used to mock up dissipative wave damping in the real plasma [32–35], thereby damping the velocity perturbations and the linear fluid equation now takes the form

$$\frac{\partial \delta v_e}{\partial t} = -\frac{e}{m_e} E - 2\gamma_d \delta v_e \ . \tag{3.31}$$

The damping rate γ_d is assumed to be significantly smaller than the wave carrier frequency, which in turn is assumed to remain close to the electron plasma frequency ω_{pe} in order to accurately represent the electric field as a single, possibly modulated, sinusoidal mode that oscillates at ω_{pe},

$$E(x,t) = A(t)\cos(kx - \omega_{pe} t) \ , \tag{3.32}$$

where the amplitude $A(t)$ is assumed to evolve slowly in time as compared with the mode oscillations, $d \ln A/dt \ll \omega_{pe}$.

The energetic electrons are described kinetically in terms of their phase space distribution function $f(x, v, t)$. Just as in the previous section f is decomposed according to Eq. (3.6). Note however that f now only represent the energetic electrons and not the bulk electrons. This means that the Poisson equation has an extra term from the energetic electrons and becomes

$$\frac{\partial E}{\partial x} = -\frac{e}{\epsilon_0}\left[\delta n_e + \int \delta f dv\right] \ . \tag{3.33}$$

The kinetic equation (3.7) governing the evolution of the distribution function f is taken as

$$\frac{\partial f}{\partial t} + v\frac{\partial f}{\partial x} - \frac{e}{m} E \frac{\partial f}{\partial v} = \mathfrak{C}\big[f\big] + S\,(v) \ . \tag{3.34}$$

The right hand side represents fast particle collisions and sources, whose combined action is to relax f towards an equilibrium distribution $F_0\,(v)$ that,

for simplicity, is taken as a constant, positive slope throughout the wave-particle resonance. It is modeled as the following combination of three operators (cf. [36])

$$\mathfrak{C}[f] + S(v) = -\beta(f - F_0) + \frac{\alpha^2}{k}\frac{\partial}{\partial v}(f - F_0) + \frac{\nu^3}{k^2}\frac{\partial^2}{\partial v^2}(f - F_0) \ . \qquad (3.35)$$

The first term is essentially a sink that relaxes the distribution function f to the equilibrium distribution at rate β. It is called the Krook operator, and is often used to mock up the effect of more challenging operators. The second term represents the effect of slowing down of the energetic electrons due to collisions with the cold particles, and is denoted collisional drag. Note that the drag operator consists of two parts. The first part acts as a constant force that slows the particles down and the second acts as a sink that preserves the equilibrium distribution function F_0. Finally, the third term in Eq. (3.35) is a velocity space diffusion operator with constant diffusion coefficient. It is included in order to represent energy space diffusion of energetic plasma particles, which is actually the dominant collisional process at low particle energy, but also to mimic the effect of stochastic scattering in localized but overlapping resonances, such as e.g. during RF heating.

All simulations in the remainder of this chapter are computed using a fully nonlinear algoritm, previously described in Ref. [37] and currently available online [38], that, given a profile for F_0 and values for γ_d, β, α and ν, solves Eqs. (3.31), (3.33) and (3.34) for the nonlinear evolution of $E(x,t)$ and $f(x,v,t)$.

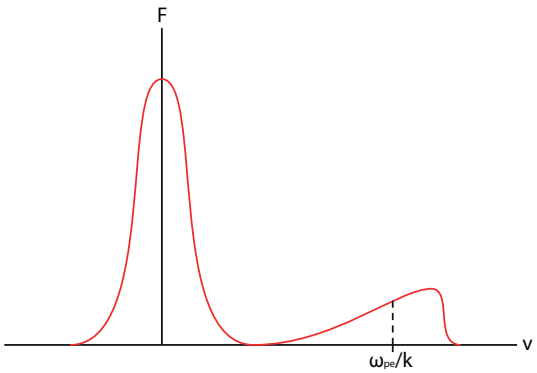

Figure 3.2: *Cartoon illustrating the bump-on-tail distribution function. The contribution from the cold electrons is treated using fluid theory and the contribution from the energetic particles is taken as a constant positive slope throughout the wave-particle resonance.*

3.4.1 Dissipative Bump-on-Tail Model Near Marginal Stability

First, we consider the collisionless, dissipationless bump-on-tail instability ($\beta = \alpha = \nu = \gamma_d = 0$). The fast particle equilibrium distribution F_0 causes the electric field amplitude to grow at a linear rate $\gamma_L \propto dF_0/dv$ due to energy released by phase mixing. The velocity width of the separatrix in Fig. 3.1 is proportional to $\sqrt{A}$ which means that as the amplitude grows the velocity width increases and passing particles on orbits just outside the separatrix become trapped. Eventually no more energy can be extracted by phase mixing and the amplitude saturates at $\omega_A = 3.2\gamma_L$ [39].

Weak dissipation is now included in the background plasma, which reduces the effective linear growth rate to $\gamma_L - \gamma_d$ and gives an instability threshold $\gamma_d = \gamma_L$. In this section we consider the *near threshold regime* where $0 < \gamma_L - \gamma_d \ll \gamma_L, \gamma_d$. Then, in Sec. 3.4.2 we mainly focus on the regime far from the instability threshold, where $\gamma_d \ll \gamma_L$.

When dissipation is present, the electric field amplitude evolution is dependent on the rate and type of collisions and on the closeness to the stability threshold. Close to the threshold the presence of Krook-type [40] and velocity space diffusion [41] on the form (3.35) result in four regimes of possible mode amplitude evolution, cf. Fig. 3.3. If the collisionality is high enough, the mode amplitude saturates at a level that reflects the closeness to threshold, i.e the saturation amplitude depends on $\gamma_L - \gamma_d$. At somewhat lower collisionality, the saturation is followed by periodic modulations, and with even less collisions the modulations become chaotic. When the collision rate is very low or even non-existent it is difficult to immediately deduce what happens.

Fig. 3.4 shows a phase space plot of the fast particle distribution at the wave-particle resonance near marginal stability in the collisionless limit. We observe the presence of coherent entities that emerge and move in phase space. Further studies of the distribution function in Fig. 3.5 reveal that the entities are regions of depletion/protrusion known as *holes* and *clumps*. There is a continuous production of holes and clumps that arise pairwise symmetrically shifted from the wave-particle resonance of the unstable bulk mode. Once formed, each pair traverses phase space in order to compensate for energy losses due to background dissipation. The convection of the holes is to higher velocities and that of the clumps to lower velocities. To a first approximation the motion preserves the value of the distribution function for the trapped particles, i.e the level of the trapped particles remains constant, so the depth/height of the hole/clump relative to the ambient distribution increases as they move. Analytically, energy conservation between the power dissipated in the cold plasma and the energy gained by the motion of the holes and clumps results in a frequency shift that initially evolves according to $\omega - \omega_{pe} \propto \pm\sqrt{t}$ [42].

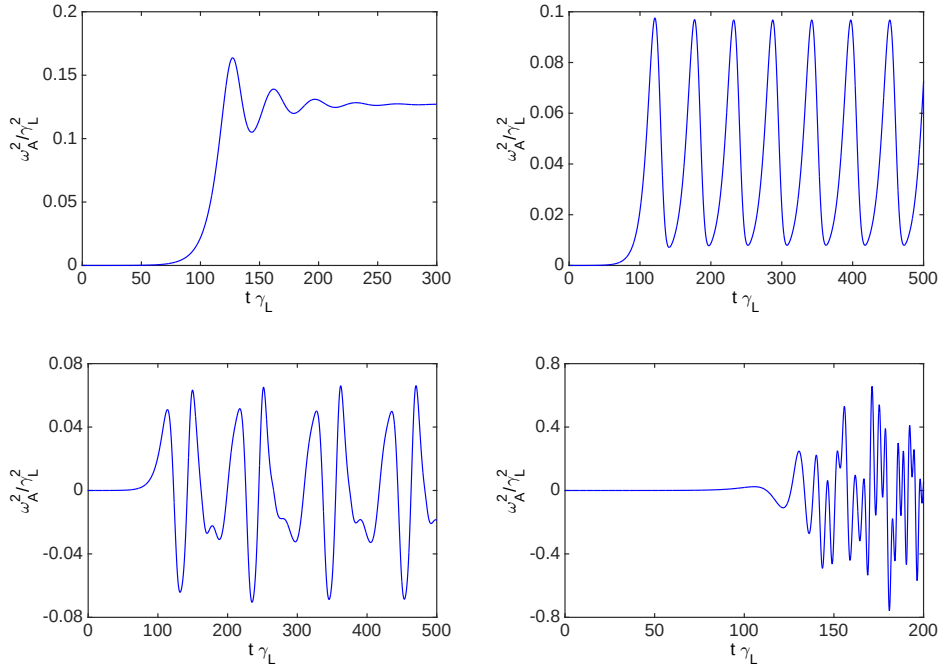

Figure 3.3: *Amplitude evolution near the instability threshold,* $\gamma_d/\gamma_L = 0.9$*, under the presence of Krook-type collisions of decreasing rate,* $\beta/\gamma_L = 0.3$*,* $\beta/\gamma_L = 0.2$*,* $\beta/\gamma_L = 0.1$ *and* $\beta/\gamma_L = 0.01$*.*

On a longer time scale fast particle collisions and other effects, such as the shape of the distribution, the dependence of γ_d on the frequency, particle inclusion/release through the separatrix via amplitude growth/decrease etc. [43], can affect the frequency sweeping. The resulting spectrogram in Fig. 3.6 shows the frequency sweeping pattern. The shifts up and down of the side bands are synched to the motion of the holes and clumps in phase space.

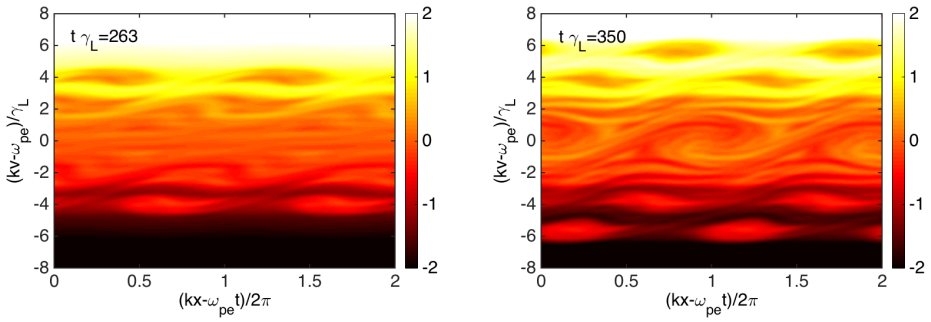

Figure 3.4: *Phase space plot of the fast particle distribution near marginal stability,* $\gamma_d/\gamma_L = 0.9$*, showing continuous production of hole-clump pairs that once formed will subsequently diverge far from the initial resonance.*

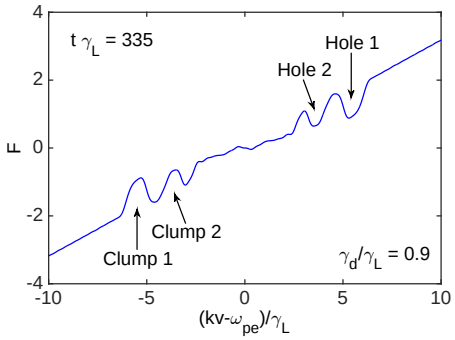

Figure 3.5: *Spatially averaged fast particle distribution in the near threshold regime. The figure displays the continuous production of hole-clump pairs that once formed will subsequently diverge far from the initial resonance.*

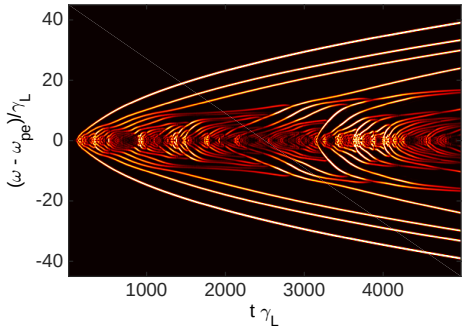

Figure 3.6: *Fourier spectrogram of the electric field amplitude showing frequency chirping near the stability threshold, $\gamma_d/\gamma_L = 0.9$.*

Contrary to diffusive and Krook-type collisions, the inclusion of drag in the form (3.35) has been shown to promote the amplitude evolution regime in Fig. 3.3d. Furthermore, it introduces an asymmetry by enhancement of the holes and their sweeping rates and depletion of the clumps. The presence of drag has an interesting effect on the frequency sweeping pattern in the spectrogram, as can be observerd in Fig. 3.7 where so called hooks and steady state holes appear [36, 43]. Similar features have, in fact, been obseved experimentally [44]. This and other observed nonlinear mode evolutions in the different amplitude regimes will be the subject of Sec. 3.5.

3.4.2 Dissipative Bump-on-Tail Model Far fom Marginal Stability

We now consider the effect of very weak dissipation, $\gamma_d/\gamma_L \ll 1$, which turns out to unlock the mysterious "spontaneous creation" [42] of the hole-clump

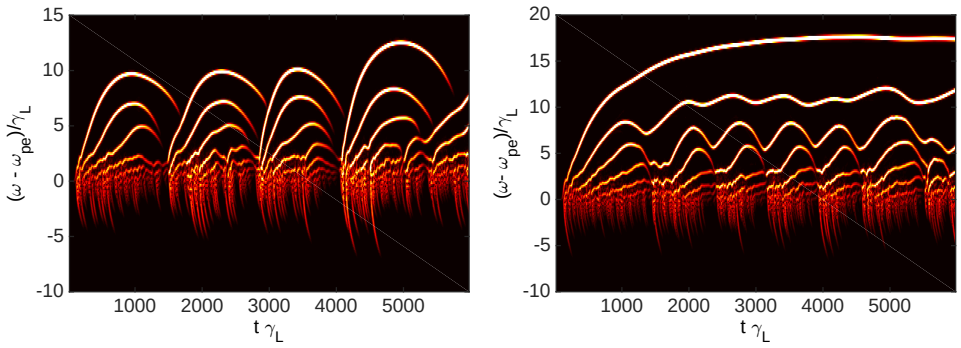

Figure 3.7: *Left: Spectrogram displaying hooked frequency sweeping. Right: Spectrogram showing a hole reaching a steady state frequency.*

formation mechanism. Fig. 3.8 shows a phase space time series of the fast particle distribution at the wave-particle resonance far from marginal stability in the collisionless limit. We observe the initial phase mixing of the resonant particles and the eye-shaped form of the saturated state. However, then dissipation kicks in and trapped particles are gradually released as the wave amplitude damps out and the separatrix shrinks and the particles begin to stream freely. This generates a nearly unmodulated phase space plateau centered at the initial resonant velocity with a velocity width somewhat smaller than the maximum width of the separatrix. The initial mode eventually damps out but notice the presence of small up- and downshifted modulations just inside the edges of the plateau in the second snapshot. These begin to grow, as seen in the third snapshot, and eventually evolve into a hole-clump pair that detatches from the plateau. In the Fourier spectrogram they correspond to frequency sweeping modes and the frequency sweeping is initiated noticeably shifted from the initial resonance.

3.5 Connection to Fast Particle Driven Instabilities in Tokamak Plasmas

Similarly as in previous sections, we consider resonant interaction between a low density population of energetic ions and a TAE. Only now, in the more complicated three dimensional geometry of a tokamak, the wave phase velocity needs to be synched with the poloidal and toroidal orbital frequencies of the energetic particles or multiples thereof. Furthermore, as previously mentioned, the linear instability growth rate depends on the gradient of the fast particle pressure. A commonly accepted idea is therefore that a gradual build-up of the energetic ion population, due to auxiliary heating or nuclear fusion reactions,

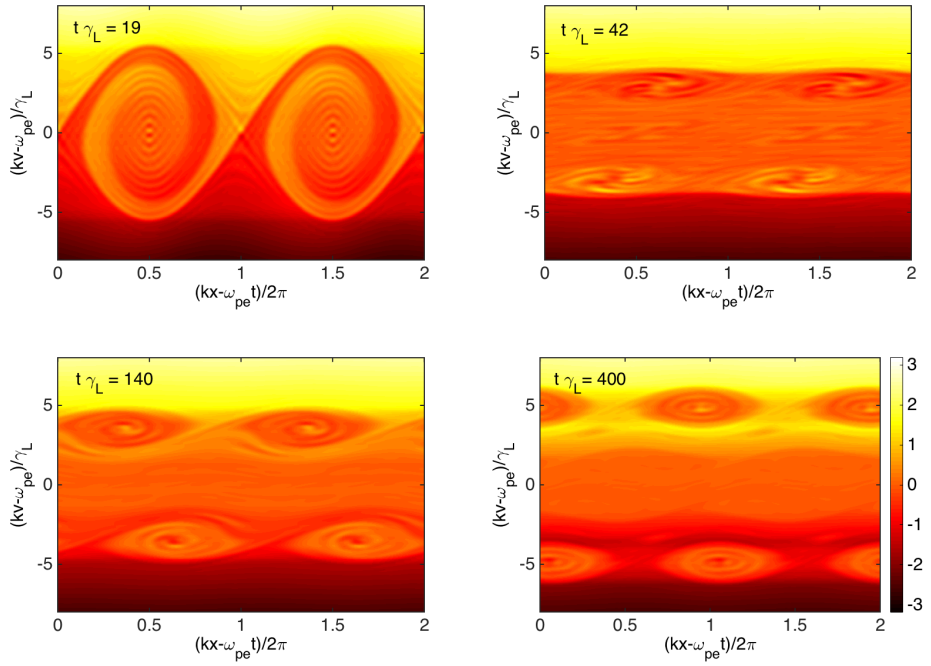

Figure 3.8: *Phase spacetime evolution of the fast particle distribution far from marginal stability,* $\gamma_d/\gamma_L = 0.1$.

eventually leads to a positive linear growth rate and mode destabilization. The energetic ions subsequently loose energy to the wave, which relaxes the gradient of the distribution toward a critical slope. This sequence of gradual build up followed by a collapse is expected to maintain the gradient just above critical level, i.e in the near threshold regime, and, historically, this idea has been supported by experimental results, cf. [10]. Recently, however, observations of bursting TAEs on ASDEX Upgrade indicate that mode destabilization may occur far from the stability threshold [45].

Experimentally, there have been many observations where the nonlinear mode evolution matches those of the numerically calculated amplitude evolutions in Fig. 3.3. The first three scenarios are illustrated in Fig. 3.9 (left), where, on JET, ICRH accelerated ions excite TAEs of different toroidal mode number. As the ICRH power is increased the initially saturated amplitude exhibits modulations and the Fourier signal splits (this phenomenon is known as *frequency splitting*), and finally blurs out as the wave evolution becomes chaotic. In relation to the bump-on-tail model, the transition from steady state to modulations of the mode amplitude occurs due to a gradual build up of the linear growth rate as the fast particle pressure builds up. The diffusive collisionality is meanwhile constant, which in turn leads to an effective decrease in collision rate [46]. A Doppler shift, due to plasma rotation from

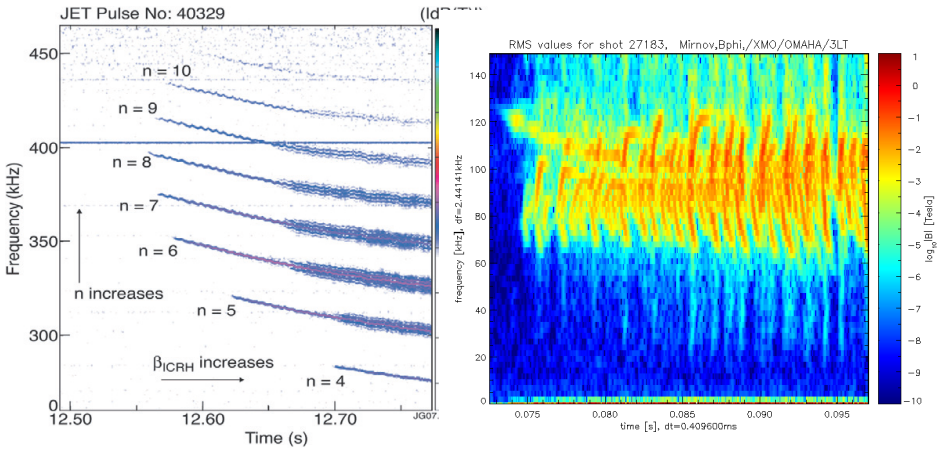

Figure 3.9: *Left: Magnetic spectrogram of JET discharge 40329 as presented in [10] displays ICHR driven Alfvén instabilities with toroidal mode numbers, which range from $n = 4$ to $n = 10$. Right: Magnetic spectrogram of MAST discharge 27183, displaying frequency sweeping TAEs.*

unidirectional NBI beams, separates the modes in frequency. The final mode evolution in Fig. 3.3, which leads to frequency sweeping signals (see Fig. 3.9), is mainly found on the spherical tokamak MAST, where the TAEs are excited by NBI generated fast ions, although, hooked frequency sweeping events have also been observed on JET [44].

4

Turbulent Particle Transport

To maximize the performance of a fusion reactor, the understanding of transport of particles and energy is important and has therefore been the subject of extensive study for decades [47]. Degradation of the confinement of a tokamak plasma comes mainly from two sources: small scale instabilites, often called microinstabilities, and large scale instabilities that are described by MHD. One important class of microinstabilites are *drift waves* driven by the free energy in gradients in temperature and density. The resulting turbulent transport is present in the plasma during normal operation conditions. As mentioned in Sec. 1.2 MHD instabilities on the other hand restrict the pressure and pressure gradients in the plasma. The ratio of particle pressure to magnetic pressure is characterized by the parameter $\beta = p/(B^2/2\mu_0)$ which is limited to a few % in most tokamak plasmas. The magnitude of β is also tied to the strength of the electromagnetic perturbations in the plasma. When analyzing drift waves in low β plasmas, it is sufficient to focus on electrostatic perturbations and neglect the magnetic field perturbations [48]. Transport models, like those used in Papers C-E, often include magnetic field perturbations in the analysis.

In this Chapter we start by presenting two types of drift waves in Sec. 4.1, the Ion Temperature Gradient mode and the Trapped Electron mode which can be understood as Rayleigh-Taylor instabilities with a dense fluid supported by a less dense fluid under the influence of gravity. Then, in Sec. 4.2 we discuss different ways to model turbulent transport in a plasma with the focus on particle transport and the resulting density profile. We present two numerical models that are used in Papers C-E to analyze particle transport as well as a transport code used to compare simulated density and temperature profiles to the corresponding experimentally obtained profiles. Finally, in Sec. 4.3 the effects of fast ions on the ITG mode turbulence is discussed.

4.1 Ion Temperature Gradient/Trapped Electron (ITG/TE) modes

Ion Temperature Gradient and Trapped Electron modes are drift waves driven by the free energy stored in the ion temperature gradient and electron density- and/or temperaure gradients, respectively. The spatial scale is typically on the order of the ion Larmor radius ($k_\theta \rho_i \sim 0.3$ for fastest growing mode) which means that it is small compared to the tokamak minor radius but large compared to the Debye length. Therefore, the Maxwell equation $\nabla \cdot \vec{E} = \rho/\epsilon_0$ is replaced to lowest order by quasineutrality $\sum_s q_s \delta n_s = 0$, where q_s is the charge and δn_s is the perturbed density of species s. The frequencies are of the order of the diamagnetic drift frequency $\omega_r \sim \omega_* = k_\theta \rho_s c_s / L_n$ (ITG $\omega_r < 0$, TE $\omega_r > 0$) where k_θ is the poloidal mode number, $c_s = \sqrt{T_e/m}$ is the ion sound speed and $L_n = -\nabla n/n$ is the density gradient length.

ITG mode

The ITG mode is commonly believed to be the most significant drift wave instability limiting confinement in current and future fusion devices [7]. A simple picture of the ITG instability in toroidal geometry is presented in Fig. 4.1. A fluctuation in temperature, δT_i, leads to a poloidal magnetic drift ($v_d \propto T_i$), causing a compression of the ion density in the poloidal direction. Assuming a periodic δT_i, δn will also be periodic and out of phase with δT_i. Quasineutrality results in a corresonding compression of the electron density which is in phase with δn_i assuming Bolzmann distributed electrons. This in turn gives rise to an electric field in the poloidal direction and a resulting radial drift. On the outboard (low field side) of the tokamak hot particles will be transported to hot regions and vice versa for the cold particles thus amplifying the original temperature perturbation and driving the instability. This propensity to drive instabilities means that is is often referred to as the *bad curvature side*. Here the poloidal variation of the density and temperature perturbations have their maxima (minima on the inside), which is referred to as ballooning.

Quantitative calculations shows that the ITG mode has a critical temperature gradient, i.e. it is unstable for $|\nabla T/T| > |\nabla T/T|_{crit}$, which is illustrated in Fig. 4.2. The existence of a threshold has also been found in experiments [49].

ETG and TE modes

Inclusion of electron dynamics leads to other drift modes such as Electron Temperature Gradient (ETG) and Trapped Electron (TE) modes. The ETG mode is analogous to the ITG mode only with spatial scales on the order of the electron Larmor radius and with electrons taking the role of the ions.

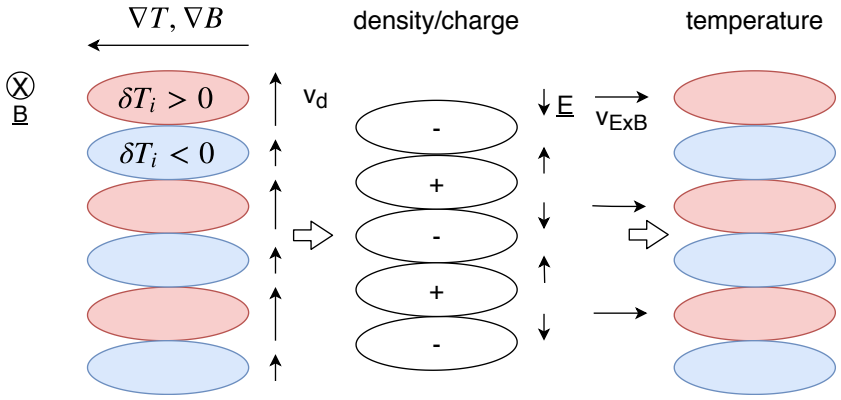

Figure 4.1: *Cartoon illustrating the ITG instability on the bad curvature side of the tokamak where $\nabla T \cdot \nabla B > 0$ (=0 at $\theta = 0$). Here hot plasma is transported to the $\delta T > 0$ regions and cold plasma to the $\delta T < 0$ regions, thus amplifying the original perturbation.*

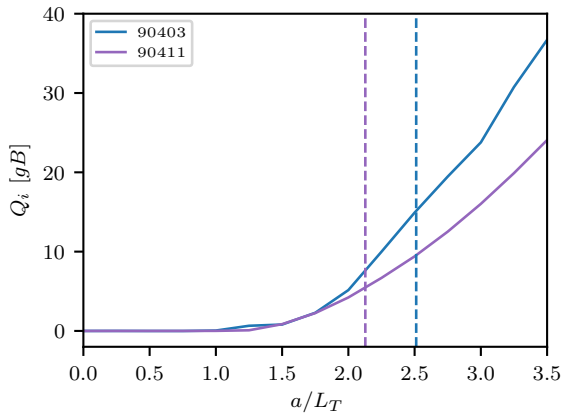

Figure 4.2: *Ion heat flux given in gyro-Bohm units as a function of normalized temperature gradient for two JET discharges. Calculated with TGLF at a single radius is the core of the plasma. The vertical dashed lines correspond to the experimental temperature gradient (set equal for electrons and ions).*

The TE mode is also similar to the ITG mode though the slow, average motion along field lines is caused by trapping as opposed to inertia for ions. Trapping effects become important if the mode frequency is below the bounce frequency. The resulting TE mode is driven by the density- or temperature gradient and stabilized by collisions. It can be the dominant instability when the ITG is weak or exist as a subdominant mode.

4.2 Transport Modelling

When analyzing particle and heat transport in a fusion plasma, numerical codes are typically used. In this section we present two *quasi-linear* transport models, the fluid model EDWM [50] and the *gyro-Landau-fluid* model TGLF [51], both of which are used in Papers C-D and D-E, respectively, to perform so called *interpretative simulations* of ITG/TE mode turbulence. The simulations are performed at a single radius in the plasma and given certain input discharge parameters, the particle and heat fluxes are calculated. The focus in this chapter is on particle transport and the resulting peaking of the density profile. In Paper E we also perform *predictive simulations* with the JETTO transport code [52] together with TGLF. Here, the profiles of density and temperature are calculated and compared to the corresponding experimentally obtained profiles when the plasma was at steady state.

4.2.1 Gyrokinetic, Gyro-fluid and Fluid descriptions

A self-consistent description of a plasma consists of the kinetic equation governing the evolution of the distribution function coupled to Maxwells' equations. Due to the complexity of this system one needs to resort to simplifications in order make it computationally feasible. In *gyrokinetic theory* the smallness of the Larmor radius compared to the typical length scale of the system is utilized. An average is performed over the fast gyromotion around the magnetic field lines which reduces the kinetic equation by one velocity space dimension. The resulting gyrokinetic equation, valid for low frequency modes ($\omega << \omega_{ci}$), together with the quasi-neutrality condition form the description for gyrokinetic turbulence modelling. Models based on gyrokinetic theory are the most accurate (in tokamak turbulence modelling) but also the most computationally expensive. The computation time can be reduced by several orders of magnitude in reduced models based on fluid theory or *gyro-fluid* theory. As mentioned in Sec. 1.3, fluid equations are obtained by taking moments of the kinetic equation. There are however, inherently kinetic effects that are not reproduced in fluid models. Some kinetic effects, such as Landau damping, are recovered in *gyro-Landau-fluid* models such as TGLF. In gyro-fluid theory on the other hand, moments are instead taken of the gyrokinetic equation.

4.2.2 Interpretative and Predictive Modelling

EDWM

EDWM is a quasi-linear fluid model used to study ITG/TE mode heat and particle transport including wavenumbers at ion scales ($k_\theta \rho_s < 1$ where $\rho_s = c_s/\omega_{ci}$ is the ion gyro radius and ω_{ci} is the ion cyclotron frequency). It is

an extended version of the Weiland drift wave model [53] and can treat an arbitrary number of species in a multi-fluid description. The model includes ion finite-Larmor-radius (FLR) effects and ion parallel motion together with electromagnetic and collisional effects. The free electrons are described by a Boltzmann distribution function in the electrostatic limit and electron FLR effects are neglected due to the scaling of the Larmor radius with mass ($\rho_e \propto \sqrt{m_e}$).

In the Weiland model each species is described by a set of fluid equations. For illustrative purposes we consider only one ion species in the electrostatic limit. Complete derivations can be found in [53, 54]. The continuity equation for ions is given by

$$\frac{\partial n_i}{\partial t} + \nabla \cdot (n_i \vec{v}_i) = 0 \ , \tag{4.1}$$

where $\vec{v}_i$ is the fluid velocity and consists of a flow parallel to the magnetic field as well as perpendicular drifts. The parallel ion motion is detemined by the parallel ion momentum equation

$$m_i n_i \frac{dv_{\parallel i}}{dt} = -eZ_i n_i \nabla_\parallel \phi - \nabla_\parallel (n_i T_i) \ , \tag{4.2}$$

where ϕ is the electrostatic potential. The perpendicular drifts are derived by the corresponding perpendicular equation. The ion energy balance equation is

$$\frac{3}{2} n_i \left(\frac{\partial}{\partial t} + \vec{v}_i \cdot \nabla \right) T_i + n_i T_i \nabla \cdot \vec{v}_i = -\nabla \cdot \vec{q}_i \ . \tag{4.3}$$

This fluid hierarchy is truncated by setting the ion heat flux ($\vec{q}_i$) equal to the diamagnetic heat flux.

Now, the fluid equations (4.1), (4.2), (4.3) are linearized for a given Fourier harmonic

$$n_i = n_i^0 + \tilde{n}_i e^{i(\vec{k} \cdot \vec{x} - \omega t)} \ , \tag{4.4}$$

same for the ion temperature and electrostatic potential, in the low frequency limit $\omega << \omega_c$. The electrons are divided into two classes: Trapped and passing. Their density perturbations are coupled through a quasi-neutrality condition

$$f_t \frac{\tilde{n}_{et}}{n_{et}} + (1 - f_t) \frac{\tilde{n}_{ep}}{n_{ep}} = \frac{\tilde{n}_i}{n_i} \ , \tag{4.5}$$

where f_t is the fraction of trapped electrons and n_{et} (n_{ep}) is the density of trapped (passing) electrons. Note that bounce effects are neglected for ions since their bounce frequency is usually much smaller than the mode frequency ($\omega_{b,i} \ll \omega$). In the collsionless limit the linearized continuity and energy equations for trapped electrons have the same form as that of the ions except that the FLR terms are neglected in the perpedicular drift. Inclusion of electron-ion

collisions result in Krook collision terms in the electron continuity and energy equations [55]. The parallel motion of trapped electrons averages to zero since their bounce frequency is much larger than the mode frequency ($\omega \ll \omega_{b,et}$) for these low frequency modes.

The linearized versions of the fluid equations for the ions together with the corresponding equations for the electrons form an eigenvalue equation which can be solved numerically for the eigenvalue $\omega = \omega_r + i\gamma$ and eigenvector consisting of the perturbed quantities. This eigenvalue equation can be reduced to a set of coupled algebraic equations by using a strong ballooning approximation (fluctuations are largest in amplitude close to $\theta = 0$). The perturbation in density δn_e is used to calculate the particle flux according to

$$\Gamma_e = \langle \delta n_e \, v_E \rangle \ , \tag{4.6}$$

where $\vec{v}_E = \vec{B} \times \nabla\phi / B^2$ is the $\vec{E} \times \vec{B}$-drift velocity and the angled brackets correspond to a flux surface average. Assuming linear relations between the field quantities ($\delta n = f(\phi, ...)$) the resulting flux is proportional to ϕ^2. Similarly, the temperature perturbation is used to calculate the heat flux. The turbulence fluctuation level (ϕ) is then determined with a modified mixing length estimate where the linear growth rate is balanced with the dominant convective $\vec{E} \times \vec{B}$ nonlinearity

$$\frac{e\phi}{T_e} \approx \frac{1}{k_r \rho_s} \frac{\gamma}{k_\theta c_s} \ , \tag{4.7}$$

and computed numerically by adding the separate transport contributions from ITG and TE modes at each wavenumber, assuming isotropic turbulence ($k_r \sim k_\theta$).

Inclusion of electromagnetic effects corresponding to *field line bending* ($\delta B_\perp$) results in an additional component to the parallel electric field

$$E_\parallel = -\nabla_\parallel \phi - \frac{\partial A_\parallel}{\partial t} \ , \tag{4.8}$$

which in turn changes the parallel momentum equation (4.2). As a result, the passing electrons are no longer Bolzmann distributed and the particle and heat transport are increased slightly from *magnetic flutter*. Here $A_\parallel$ is the parallel component of the vector potential $\vec{A}$ given by Ampéres law $\vec{B} = \nabla \times \vec{A}$. Note that parallel magnetic field perturbations ($\delta B_\parallel$), which are negligable in low β plasmas, are neglected in the Weiland model.

Trapped-gyro-Landau-fluid model (TGLF)

The trapped-gyro-Landau-fluid model (TGLF) is the latest generation gyro-Landau-fluid model. Like its predecessors, it includes kinetic effects such as

Landau damping, though TGLF unifies trapped and passing particles to a single set of equations. Also, it treats electrons, main and fast ions and impurities as well as electron-ion collisions [56] and electromagnetic effects in a shaped Miller geometry [57]. It is a quasi-linear model where a system of moments of the gyrokinetic equation is solved for the linear eigenmodes of trapped ion and electron modes (TI, TE), ion and electron temperature gradient (ITG, ETG) modes and electromagnetic kinetic ballooning (KB) modes. The quasi-linear fluxes are calculated for the full spectrum of linear modes, i.e including both ion scales ($0.1 < k_\theta \rho_s < 1$) and electron scales ($1 < k_\theta \rho_s < 24$). Since TGLF is a quasi-linear model, the turbulent saturation level needs to be determined. The saturated potential is modeled to fit a database of nonlinear gyrokinetic simulations. In Papers D-E, TGLF simulations are performed with the spectral shift saturation model SAT1, presented in [58]. With TGLF-SAT1 zonal flow mixing rather than shearing is the main saturation mechanism. Also, some coupling between the ion scales and electron scales is included as well as a radial wavenumber spectrum for each k_θ. With TGLF-SAT1, effects such as enhancement of electron scale energy transport by streamers and the upshift of the effective critical ion temperature gradient (Dimits shift) are captured. Since ITER plasmas will be close to marginal stability in the core, proper capturing of such nonlinear effects may be important to predict the possible performance of ITER.

Density Peaking

In general, the quasi-linear electron particle flux, given by (4.6) can be expressed as [59]

$$\Gamma_e = \frac{n_e}{a}\left(D\frac{a}{L_{n_e}} + aV_{th} + aV_p \right) , \tag{4.9}$$

where a positive Γ_e corresponds to an outward flux. Here n_e is the electron density and a is the minor radius of the tokamak. The first term inside the bracket is the outward diffusive contribution, given by the diffusivity coefficient D and the normalized electron density gradient ($a/L_{n_e} = -a\nabla n_e/n_e$). The second and third terms represent the convection, also known as a "pinch" that can be inward or outward. It consists of a thermal pinch proportional to the electron temperature gradient and a "pure" convection, dominated by the so called curvature pinch. The diffusion and convection coefficients (D, V_{th}, V_p) have been extensively studied (see e.g. [59–62]) and are themselves dependent of density- and temperature gradients so Eq. 4.9 is not linear, though it is a practical physical decomposition.

In steady state, the particle flux in Eq. 4.9 is balanced by the external

source and the resulting density peaking (from Eq. (4.13a)) becomes [63]

$$\frac{a}{L_{n_e}} = -\frac{aV_{tot}}{D} + \frac{a}{Dn_eV'\langle|\nabla\rho_t|^2\rangle}\int_0^{\rho_t} SV'd\rho \ , \tag{4.10}$$

were $V' = \partial V/\partial\rho_t$ and V_{tot} is the total convective velocity. The first term on the right hand side in Eq. 4.10 is the zero flux peaking factor (PF), studied in Papers C-E, and defined as the local density peaking at zero particle flux in steady state i.e. with the source term zero. The second term is the contribution from the source inside ρ_t to the peaking. The sign of the particle pinch determines the sign of the peaking factor. A positive peaking factor corresponds to a peaked density profile while a negative one to a hollow density profile (neglecting influence of the source), hence the name peaking factor. Note that the particle flux and density gradients for the plasma species are restricted by ambipolarity

$$\sum_s q_s\Gamma_s = 0 \ , \tag{4.11a}$$

and quasi-neutrality

$$\sum_s q_s n_s = 0 \ , \tag{4.11b}$$

where q_s is the charge. Taking the radial derivative of (4.11b) result in a quasi-neutrality condition on the density gradients

$$\sum_s q_s A_s \frac{a}{L_{n_s}} = 0 \ , \tag{4.12}$$

where $A_s = n_s/n_e$ is the density fraction of species s. Since the electron density profile is the the one measured in the experiment, the focus in Papers C-E is on electron particle transport and additional species, such as impurities or fast ions, are bound by the conditions in Eqs. (4.11) and (4.12).

JETTO Transport Code

Predictive simulations using transport codes can evolve the plasma profiles $(n, T, J, v_{tor}..)$ and equilibrium self-consistently. Since the experimental discharges studied in Paper E are in steady state, the predictive simulations are used to assess the performance of a theoretical transport model in comparison with experimental data. In this section, we present an overview of the JETTO transport code that, together with TGLF, is used for predictive simulations in Paper E. Primarily, JETTO solves the particle and energy balance equations. Given a set of input data, JETTO calculates the profiles under the influence of transport and sources and sinks of particles and energy. It has a modular structure where the input required comes partially from experimentally obtained

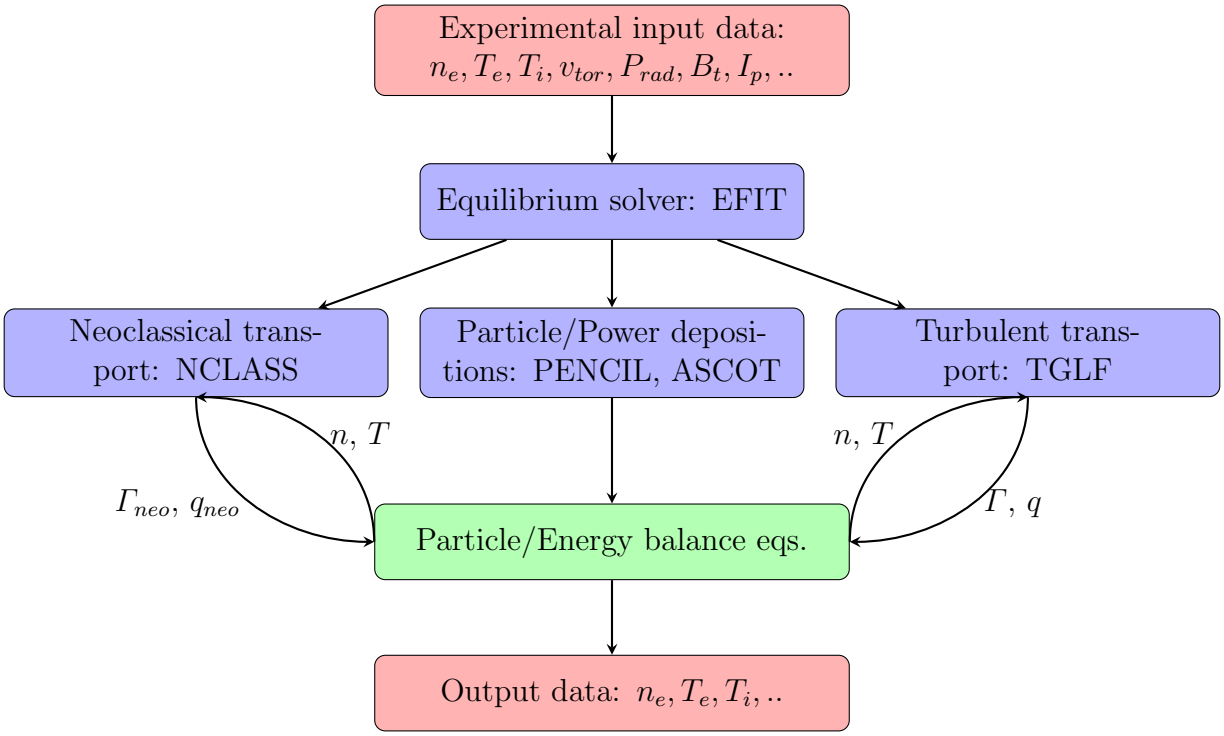

Figure 4.3: Flowchart illustrating the modular structure of the JETTO simulations performed in Paper E for discharges in steady state.

data and partially from calculated quantities provided by separate packages. A structure over the modular setup used for the predictive simulations in Paper E is presented in a flowchart in Fig. 4.3.

Typical experimental input data consist of

- Electron density and temperature from High Resolution Thompson Scattering (used as initial profile)
- Toroidal rotation profile (and possibly ion temperature) from Charge Exchange Recombination Spectroscopy (used as initial profile)
- Profile of radiated power from bolometry
- Plasma current from magnetic field measurements
- Effective charge from spectroscopy

A splitting technique is applied to calculate the MHD equilibrium configuration separate from the transport equations. Given a set of experimental input data, the EFIT code [64] calculates the magnetic equilibria at steady state by solving the ideal MHD force balance equation 2.8. The radial variable used in JETTO to label the resulting flux surfaces is $\rho_t = \sqrt{\psi_t/\psi_a}$ where ψ_t is the

toroidal flux given by Eq. (2.9b) and ψ_a is the toroidal flux evaluated at the *last closed flux surface*. For the resulting magnetic configuration, the plasma profile is divided into zones and a flux surface average is performed. Then the particle and energy balance equations are solved. For species j they are given by [52]

$$\frac{\partial n_j}{\partial t} + \frac{1}{V'}\frac{\partial}{\partial \rho_t}\left(V' \Gamma_j\right) = S_j \ , \tag{4.13a}$$

$$\frac{3}{2}\frac{\partial P_j}{\partial t} + \frac{1}{V'}\frac{\partial}{\partial \rho_t}\left[V'\left(\langle \vec{q}_i \cdot \nabla \rho_t \rangle + \frac{3}{2} T_j \Gamma_j\right)\right] = Q_j \ . \tag{4.13b}$$

Here, the angled brackets correspond to a flux surface average and the time derivatives are evaluated at constant ρ_t. In Paper E, S_j represents the NBI particle source and Q_j the corresponding power gain and losses due to the NBI, electron-ion thermal equilibration, radiation and, for electrons, Ohmic heating. The heat and particle deposition profiles from the NBI particle source are calculated in a separate package, such as PENCIL [65] or ASCOT (ref). Fig. 4.4 illustrates an example of the deposition profiles for the JET discharge 87420. Particle and power deposition profiles from the NBI are constant throughout the simulation. The remaining terms are evaluated at each time step and presented at the end of the simulation in Fig. 4.4. A transport model, such as TGLF, is used to calculate the flux surface averaged particle (Γ_j) and heat (q_j) for each timestep. Finally, the corresponding diffusivities from neoclassical transport are calculated with NCLASS [66]. Profiles of n_e, T_e and T_i are determined at each time step with boundary conditions at $\rho_t = 0.8$ set fixed by the experiment and the derivative of the profile set to zero at the center. When the experimentally determined profiles are taken as initial profiles, steady state is usually reached after $\sim$ 1s.

Fig. 4.5 shows the result of two predictive simulations of one of the discharges in Paper E, one with and one without the NBI particle source. Experimental profiles are in black and the simulated profiles in color in the left figures. The two figures on the right show time series at $\rho_t = 0.56$. Electron density is shown both with and without the particle source and the difference between the two corresponds to the influence of the source on the density peaking (second term in Eq. 4.10). The experimental ion and electron temperatures are approximately equal. Predicted temperatures are shown only with the source.

4.3 Fast Ion Effects on ITG mode Driven Turbulence

In addition to possibly destabilizing fast particle driven instabilites, such as Alfvén waves, the presence of fast particles also affects ITG driven turbulent

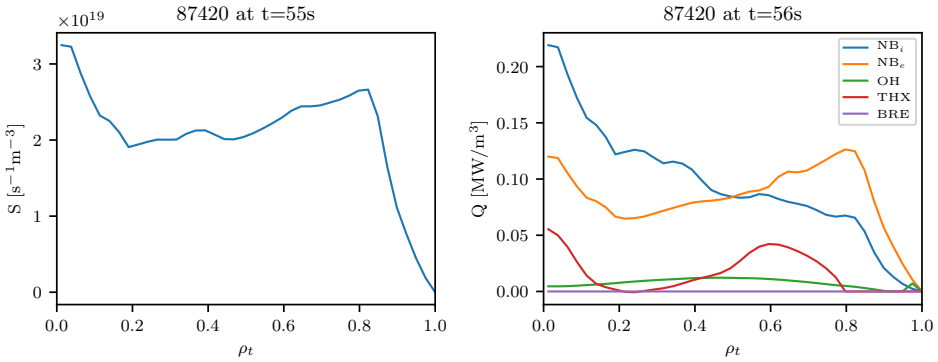

Figure 4.4: *Left: Particle deposition profile for JET discharge 87420, shown at the initial time step and kept constant throughout the simulation. Right: Power deposition profiles shown at the end of the simulation for the same discharge. The contribution from the NBI to the ions and electrons (NB_i and NB_e) are kept constant throughout the simulations. The remaining terms are evolved and represent Ohmic heating (OH), e-i thermal equilibration (THX) and finally Bremstrahlung radiation (BRE).*

transport. Modelling efforts show that the inclusion of a fast ion species has a stabilizing influence on ITG driven turbulence through a number of different effects: First, the inclusion of an additional ion species affects the main ion density and density gradient due to quasi-neutrality (4.11b) and (4.12). This is known as *dilution* and, since the main ions are responsible for the drive of ITG turbulence, it has a stabilizing influence [16]. Fast ions also increase the total thermal pressure in the plasma which in turn increases β. As long as the mode is ITG like, an increase in β reduces the linear mode growth rate which has a direct impact on the turbulence saturation level [48]. An additional stabilizing effect from a higher β comes from an increase of the radial shift of the magnetic flux surfaces toward the outboard side of the tokamak, known as a *Shafranov shift*. A larger Shafranov shift stabilizes curvature and ∇B driven instabilites such as the ITG mode [15]. Finally, using nonlinear gyrokinetic simulations, the inclusion of fast ions has been shown to result in electromagnetic stabilization of ITG driven turbulence due to suprathermal pressure gradients [11, 14].

4.3.1 Fast Ion Distribution Function

Fast ions can be characterized by their distribution in phase space. If we only consider the pitch angle averaged distribution function the appropriate Fokker-Planck equation reduces to one dimension in velocity space. For NBI

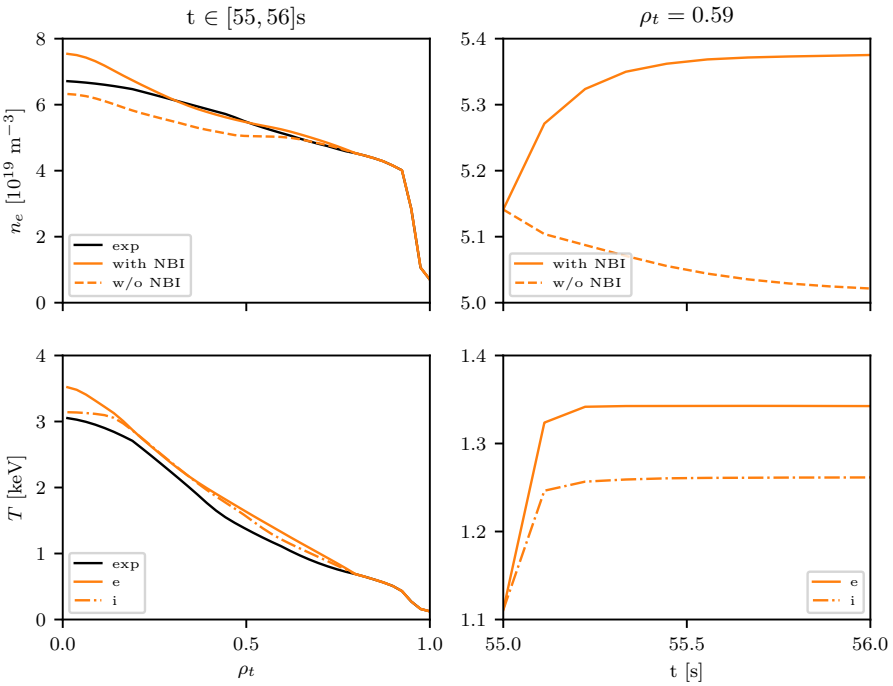

Figure 4.5: *Left: Electron density and electron and ion temperature profiles for discharge 87420. Experimental profiles in black correspond to inital time 55s and the ones in color to the simulated profiles at 56s. Density profiles show both with and without NBI source and temperature profiles with NBI. At 55s the electron and ion temperature profiles are equal. Right: Time series evaluated at $\rho_t = 0.59$ to illustrate steady state.*

generated ions and fusion born α particles we obtain,

$$\frac{\partial f}{\partial t} = C(f) + \frac{S_0}{4\pi v_0^2}\delta(v_0 - v) = 0 \ . \tag{4.14}$$

Here $C(f)$ is the fast ion collision operator and S_0 is the rate at which the fast ions are born, each with velocity v_0, where we have approximated the source to be mono-energetic. The collision operator is often divided into dynamical friction (drag) and velocity space diffusion. For NBI generated fast ions and fusion generated alpha particles dynamical friction dominates over velocity space diffusion. Neglecting self-interactions and assuming that the thermal electrons and ions have Maxwellian distribution functions, the collision oper-

ator, simplifies to (see e.g. [67])

$$C(f) = \frac{1}{\tau_s v^2}\frac{\partial}{\partial v}\left[(v^3 + v_c^3)f\right] , \tag{4.15}$$

where

$$\tau_s = \frac{3\pi^{3/2} m_e m_f \epsilon_0^2}{n_e Z_a^2 e^4 \ln\Lambda} v_{te}^3 , \tag{4.16}$$

is the slowing down time [67], and v_c is a critical velocity where the ions and electrons contribute equally to the slowing down of the fast ion. It is given by

$$v_c^3 = \frac{3\sqrt{\pi}}{4}\frac{m_e}{n_e}\frac{Z_i^2 n_i}{m_i} v_{te}^3 . \tag{4.17}$$

Here $\ln\Lambda$ is the so called *Coulomb logaritm* and is related to the average deflection angle in the collision ($\ln\Lambda \sim 10-20$ in a fusion plasma which corresponds to small angle deflections [68]) and v_{te} is the electron thermal velocity. For velocities larger than v_c the electron drag dominates over the ion drag. If we are considering fusion born α-particles, which are born with velocities much greater than this critical velocity, this explains why most of the fusion power from the α-particles goes to heating of the electrons rather than the ions. In steady state, the resulting *slowing down distribution* takes the form

$$f = \frac{S_0\tau_s}{4\pi}\frac{1}{v^3 + v_c^3} H(v_0 - v) , \tag{4.18}$$

where H is the Heaviside step function. The fast ion density can be calculated as

$$n_f = \frac{S_0\tau_s}{4\pi}\int_0^{v_0} \frac{1}{v^3 + v_c^3} 4\pi v^2\, dv = \frac{S_0\tau_s}{3}\ln\left(1 + \frac{v_0^3}{v_c^3}\right) , \tag{4.19}$$

and the energy

$$\begin{aligned} w_f &= \frac{m_f}{2}\frac{S_0\tau_s}{4\pi}\int_0^{v_0} \frac{v^2}{v^3 + v_c^3} 4\pi v^2\, dv = ... \\ &= \frac{m_f S_0\tau_s}{2}\left\{\frac{v_0^2}{2} + \frac{v_c^2}{3}\left[\ln\left(1 + \frac{v_0}{v_c}\right) - \frac{1}{2}\ln\left(1 - \frac{v_0}{v_c} + \frac{v_0^2}{v_c^2}\right)\right.\right. \\ &\left.\left. - \sqrt{3}\arctan\left(\frac{2\frac{v_0}{v_c} - 1}{\sqrt{3}}\right) - \frac{\pi}{2\sqrt{3}}\right]\right\} . \end{aligned} \tag{4.20}$$

The fast ion temperature is taken as

$$T_f = \frac{w_f}{n_f} , \tag{4.21}$$

which for fusion generated alpha particles fulfilling $v_0 >> v_c$ only has a very weak spatial variation. The logaritmic variation of T_f with radius, through v_c,

means that it varies relatively little also for NBI injected ions as illustrated in Fig. 4.6. The profiles are calculated with the PENCIL code when the experiment was at steady state. Note that the temperature profile is basically flat, $a/L_{n_f} > a/L_{T_f}$. The opposite tends to be true for ICRH heated discharges [67].

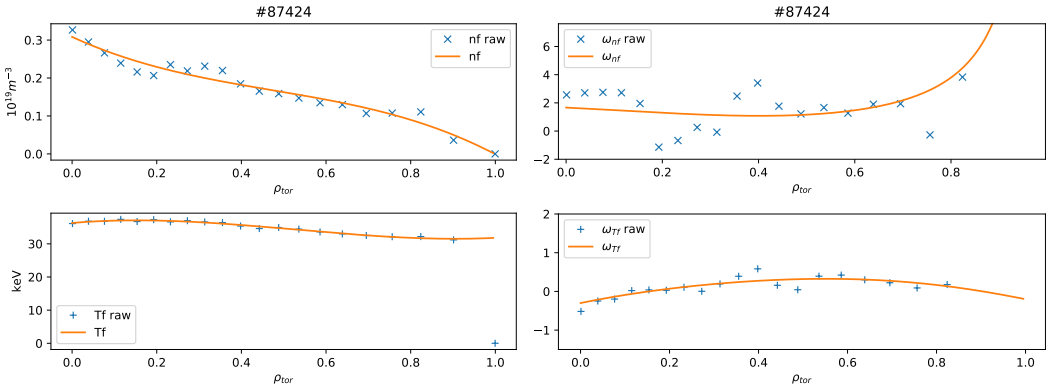

Figure 4.6: *Fast ion data for the NBI heated discharge 87424 (analyzed in Paper D) at $\rho_t = 0.6$, calculated with the PENCIL code. Here $\omega_{nf} = a/L_{nf}$ and $\omega_{Tf} = a/L_{Tf}$.*

When modelling the effect of fast ions on transport, most transport models are restricted to a Maxwellian distribution function. In [69] the equivalent Maxwellian temperature of a slowing down distribution was calculated by matching velocity moments of the distribution functions. Recently, the GENE code [70] was extended to allow for an arbitrary fast ion distribution functions [71] which showed a lack of sensitivity to the fast ion distribution for NBI generated fast ions. The stabilizing effect was less strong with a realistic fast ion distribution but still substantial.

5

Brief Summary of Included Papers

In Papers A and B we use the electrostatic one-dimensional bump-on-tail model, presented in Sec. 3.4, to study single, isolated fast particle driven instabilities. In this model a low density beam of fast electrons is represented as a small "bump" at the tail of the background electron distribution function. As mentioned in Chapter 3, particle motion can be effectively one-dimensional in the vicinity of single, isolated resonances if expressed in action angle variables. Therefore, a qualitative understanding of nonlinear wave-particle interaction can be gained with a one-dimensional model like the bump-on tail model. In Paper A, we consider a single, isolated TAE mode in the presence of a low density population of energetic ions. After the initial exponential growth of the mode amplitude, the nonlinear TAE evolution can be analyzed using the bump-on tail model, cf. [41]. We study the so called bursting type eigenmodes, where the mode develops highly persistent sidebands with time dependent frequencies. As their frequencies evolve in time, they also move radially through the plasma. This motion in calculated in Paper A by recognizing that fast particles trapped in resonance with the wave field will follow the mode locus radially, while executing their guiding center and Larmor gyration orbits.

In Paper B we study the creation and evolution of phase space structures known as holes and clumps in the dissipative bump-on-tail model far fom marginal stability. We follow and expand Ref. [72] in order to substantiate the idea of an intermediate phase space plateau as a hole-clump breeding ground via destabilization of *edge modes*. We employ linear and nonlinear stability analysis to investigate the role of fast particle collisions and sources and also relaxation of the edge gradients of the plateau. It turns out that it is not the existence of a plateau that determines whether holes and clumps appear but rather the effect of collisions on that plateau. Krook-type collisions and velocity space diffusion inhibit hole-clump formation mainly by relaxation of

the plateau that in turn reduces the growth rates of the edge modes. An asymmetry of the growth rates of the holes and clumps, favoring the hole over the clump, in the presence of drag collisions is due to convection of the entire plateau down along the ambient slope distribution.

Next, in Papers C-E, particle and heat transport from ITG/TE mode driven turbulence is studied. Focus is on particle transport ($\Gamma = -D\nabla n + nV$) which together with the particle sources form a balance that determines the peaking of the density profile according to Eq. (4.13a). The density profile in turn is important for the performance of a fusion device since, for instance, fusion power scales with density squared.

First, in Paper C we consider regions of hollow density profiles using fluid as well as local and global gyrokinetic simulations. Hollow density profiles may occur locally in connection with pellet fuelling where the ITG mode driven turbulence is responsible for the transport of the pellet towards the center. The positive density gradient region, created by the pellet, could potentially stabilize the turbulence or change the relation between convective and diffusive fluxes, thereby reducing the turbulent transport of particles towards the centre which would weaken the efficiency of pellet fuelling. The effect of fast ions and nonlocal effects are investigated. In the simulations, typical tokamak parameters are used based on the Cyclone Base Case [73] that corresponds to an ITG dominated H-mode discharge. Fast ions are modelled with a Maxwellian background distribution in both the fluid and gyrokinetic model and parameter scalings with fast ion fraction, temperature and corresponding gradients are considered. High β and inclusion of fast ions tends to be stabilizing and could thus possibly pose problems for pellet fuelling. Also, when nonlocal effects are important a positive density gradient can lead to higher transport than in the flux tube predictions.

Then, in Papers D and E we study the effect of the NBI particle source on density peaking. To evaluate the importance of the NBI particle source for the density peaking in present experiments and improve the extrapolation to ITER (with lower collisionality), dedicated dimensionless collisionality scaling experiments have been performed in various scenarios at JET [74]: L-mode with Carbon wall, deuterium, hydrogen and higher beta H-mode in ILW. In the experiments, the collisionality was varied while other key dimensionless parameters like beta, normalized gyroradius, safety factor, magnetic shear, normalized temperature gradient and Z_{eff} were kept constant within experimental error bars. The large range in collisionality in the different operating scenarios, performed in both Carbon wall and ITER-Like wall (ILW) JET plasmas, and the well matched dimensionless parameters obtained within each scan in both deuterium and hydrogen plasmas, makes them ideal for theoretical investigations of the role of the NBI particle source versus the turbulent pinch for density peaking. The 12 discharges are also very well suited for validation

studies of transport models.

In Paper D, the effect of fast ions on density peaking was analyzed for the lowest collisionality L-mode and deuterium H-mode discharges at a single radial position in the core of the plasma using three different transport models (EDWM, TGLF and linear and nonlinear GENE). In the simulations, fast ions are included as a separate species with a Maxwellian background distribution and their effect on the density peaking is studied. Fast ion driven instabilities are not included. Inclusion of fast ions affects the equilibrium plasma parameters such as safety factor, magnetic shear and flux surface shape, as mentioned in Sec. 4.3. In Paper D they are kept fixed in order to isolate the effect of fast ions on the ITG mode. The main ion (or electron) density and density gradients are adapted to keep quasineutrality. In general, the reduced models reproduce the result of the gyrokinetic model qualitatively. All three models agree that inclusion of a fast ion species has a stabilizing influence on the ITG mode and reduces the peaking of the main ion and electron density profiles in the absence of sources.

In Paper E, interpretative simulations at a fixed radial position are combined with predictive JETTO simulations of temperatures and densities, using the TGLF transport model for all 12 JET discharges in the four collisionality scans. In the predicitve modelling, the electron density profile and the electron and ion temperature profiles were evolved until steady state was reached while the rotation and safety factor profiles were taken from the experiment. Predictive simulations were performed with and without the NBI particle source, as described in Sec. 4.2.2, including electromagnetic effects, collisions and rotation. Both interpretative and predicitve simulations agree that most of the peaking in the L-mode discharges is from the turbulent inward pinch while for the H-mode discharges, the NBI source is significant for the peaking, in agreement with the experimental conclusions. The influence of impurities was evaluated for the low collisionality L-mode discharge by including 2% Carbon which had a negligible effect on the density peaking. Rotation was found to have a small influence on all discharges except the low collisionality higher beta H-mode discharge. In general, TGLF reproduced the profiles well with rms errors below 6% for the density (except one discharge) and an average of 8.4% and 13.4% for the ion and electron temperature, respectively. A natural extension of the work performed in Paper E is to analyze the next set of experimental discharges planned in tritium and at even lower collisionality which will be even more ITER relevant.

Bibliography

[1] U. S. Energy Information Administration, *www.eia.doe.gov*, Jan 4, 2016

[2] J. Wesson, *Tokamaks*, Oxford University Press, Oxford, 3rd edition (2004)

[3] CCFE Culham Center Fusion Energy, *www.ccfe.ac.uk*, Jan 26, 2016

[4] International Thermonuclear Experimental Reactor, *www.ITER.org*, Jan 4, 2016

[5] J. D. Lawson, *Some Criteria for a Power Producing Thermonuclear Reactor*, Phys. Soc. B **70**, 6 (1957)

[6] P. C. Liewer, *Measurements of mictroturbulence in tokamaks and comparisons with theories of turbulence and anomalous transport*, Nucl. Fusion **25** 5:543 (1985)

[7] E. J. Doyle, W. A. Houlberg, Y. Kamada et al *Plasma confinement and transport*, Nucl. Fusion 47(6):S18 (2007)

[8] A. Fasoli, C. Gormenzano, H. L. Berk, *et al*, *Progress in the ITER Physics Basis, Chapter 5: Physics of energetic ions*, Nucl. Fusion **47**, S264 (2007)

[9] W. W. Heidbrink and G. J. Sadler, *The Behavior of Fast Ions in Tokamak Experiments*, Nucl. Fusion **34** (4), 535 (1994)

[10] S. E. Sharapov, B. Alper, H. L. Berk, *et al*, *Energetic particle instabilities in fusion plasmas*, Nucl. Fusion **53**, 104022 (2013)

[11] J. Citrin, F. Jenko, P. Mantica, *et at*, *Nonlinear stabilization of tokamak microturbulence by fast ions*, PRL **111**, 155001 (2013)

[12] M. Liljeström, *Low frequency electrostatic instabilities in a toroidal plasma with a hot ion beam*, Nucl. Fusion **30**, 2611(1990)

[13] G. Wilkie, A. Iantchenko, I. G. Abel, *et at*, *First principles of modelling the stabilization of microturbulence by fast ions*, Nucl. Fusion **58** 082024 (2018)

[14] J. Garcia, C. Challis, J. Citrin, *et at*, *Key impact of finite-beta and fast ions in core and edge tokamak regions for the transition to advanced scenarios*, Nucl. Fusion **55**, 053007 (2015)

[15] C. Bourdelle, G. T. Hoang, X. Litaudon, *et at*, *Impact of the α parameter on the microstability of internal transport barriers*, Nucl. Fusion **45**, 110 (2005)

[16] C. Holland, L. Schmitz, T. L. Rhodes, *et al*, *Advances in validating gyrokinetic turbulence models against L- and H-mode plasmas*, Phys. Plasmas **18**, 056113 (2011)

[17] J. P. Freidberg, *Ideal magnetohydrodynamic theory of magnetic fusion systems*, Rev. Mod. Phys. **54** (3), 801 (1982)

[18] M. N. Rosenbluth, H. L. Berk, J. W. Van Dam and D. M. Lindberg, *Mode structure and continuum damping of high-n toroidal Alfvén eigenmodes*, Phys. Fluids B **4** (7), 2189 (1992)

[19] H. L. Berk, J. W. Van Dam, Z. Guo and D. M. Lindberg, *Continuum damping of low-n toroidicity induced shear Alfvén eigenmodes*, Phys. Fluids B **4** (7), 1806 (1992)

[20] L. Chen and A. Hasegawa, *Plasma heating by spatial resonance of Alfvén wave*, Phys. Fluids **17** (7), 1399 (1974)

[21] C. Z. Cheng, L. Chen and M. S. Chance, *High-n Ideal and Resistive Shear Alfvén Waves in Tokamaks*, Ann. Phys. **161**, 21 (1985)

[22] B. N. Breizman and S. E. Sharapov, *Energetic particle drive for toroidicity-induced Alfvén eigenmodes and kinetic toroidicity-induced Alfvén eigenmodes in a low-shear tokamak*, Plasma Phys. Control. Fusion **37**, 1057 (1995)

[23] G. T. A. Huysmans, J. P. Goedbloed and W. O. K. Kerner, p. 371 in *Proc. of the CP90 Conference on Computational Physics, Amsterdam*, World Scientific, Singapore, (1991)

[24] A. B. Mikhailovskii, G. T. A. Huysmans, W. O. K. Kerner and S. E. Sharapov, *Optimization of Computational MHD Normal-Mode Analysis for Tokamaks*, Plasma Phys. Rep. **23** (10), 844 (1997)

[25] T. Fülöp, M. Lisak, Ya I Kolesnichenko and D. Andersson, *Finite orbit width stabilizing effect on toroidal Alfvén eigenmodes excited by passing and trapped energetic ions*, Plasma Phys. Control. Fusion **38** (1996)

[26] S. E. Sharapov, *Fast Particle Driven Alfvén Eigenmodes in Tokamaks*, Fusion Science and Technology **57** 156 (2010)

[27] G. Y. Fu and J. W. Van Dam, *Excitation of the toroidicity-induced shear Alfvén eigenmode by fusion alpha particles in an ignited tokamak*, Phys. Fluids B **1** (10), 1949 (1989)

[28] B. V. Chirikov *A universal instability of many-dimensional oscillator systems* Phys. Rep **52** No. 5 (1979)

[29] L. D. Landau, *On the vibrations of the electronic plasma*, J. Physics **10**, 25 (1946)

[30] G. Arfken, H. Weber and F. Harris, *Mathematical methods for physicists*, Academic Press, Oxford, 7th edition (2013)

[31] F. Chen, *Introduction to plasma physics*, Plenum Press, New York (1974)

[32] R. Betti and J. P. Freidberg, *Stability of Alfvén gap modes in burning plasmas*, Phys. Fluids B **4** (6), 1465 (1992)

[33] N. N. Gorelenkov and S. E. Sharapov, *On the collisional damping of TAE-modes on trapped electrons in tokamaks*, Phys. Scripta **45**, 163 (1992)

[34] M. N. Rosenbluth, H. L. Berk, J. W. Van Dam and D. M. Lindberg, *Continuum damping of high-mode-number toroidal Alfvén waves*, Phys. Rev. Lett. **68** (5), 596 (1992)

[35] R. M. Nyqvist and S. E. Sharapov, *Asymmetric radiative damping of low shear toroidal Alfvén eigenmodes*, Phys. Plasmas **19**, 082517 (2012)

[36] M. K. Lilley, B. N. Breizman and S. E. Sharapov, *Effect of dynamical friction on nonlinear energetic particle modes*, Phys. Plasmas **17**, 092305 (2010)

[37] M. K. Lilley, B. N. Breizman and S. E. Sharapov, *Destabilizing effect of dynamical friction on fast-particle-driven waves in a near-threshold nonlinear regime*, Phys. Rev. Lett. **102**, 195003 (2009)

[38] M. K. Lilley (2010), source code available from https://github.com/mklilley/BOT

[39] See National Technical Information Service Document No. AD730123 PGG-93, B. Fried, C. Lui, W. Means and R. Sagdeev, University of California Report No. AD730123 PGG-93, 1971. Copies may be ordered from the National Technical Information Service, Springfield, Virginia 22161

[40] H. L. Berk, B. N. Breizman and M. S. Pekker, *Nonlinear dynamics of a driven mode near marginal stability*, Phys. Rev. Lett. **76** (8) 1256, (1996)

[41] B. N. Breizman, H. L. Berk, M. S. Pekker, *et al*, *Critical nonlinear phenomena for kinetic instabilities near threshold*, Phys. Plasmas **4**(5), 1559 (1997)

[42] H. L. Berk, B. N. Breizman and N. V. Petviashvili, *Spontaneous hole-clump pair creation in weakly unstable plasmas*, Phys. Lett. A **234** 213 (1997)

[43] R. M. Nyqvist and B. N. Breizman, *Modeling of long range frequency sweeping for energetic particle modes*, Phys. Plasmas **20**, 042106 (2013)

[44] H. L. Berk, C. J. Boswell, D. Borba, , *Explanation of the JET n = 0 chirping mode*, Nucl. Fusion **46**, S888 (2006)

[45] P. Lauber, M. Schneller, X. Wang, *et al*, *Kinetic models for energetic particle physics in tokamaks - verifications, validation and predictions for ITER* Theory of Fusion Plasmas: Joint Varenna-Lausanne International Workshop, Villa Monastero, Varenna, Italy, September 1 – 5, 2014

[46] W. Kerner, D. Borba, S. E. Sharapov, *et al*, *Theory of Alfvén eigenmode instabilities and related alpha particle transport in JET deuterium-tritium plasmas*, Nucl. Fusion **38** 9 (1998)

[47] L. A. Artsimovich *Tokamak devices*, Nucl. Fusion **12** 215 (1972)

[48] R. Balescu, *Aspects of Anomalous Transport in Plasmas*, Bristol: IOP Publishing (2005)

[49] P. Mantica, D. Strintzi, T. Tala *et al*, *Experimental study of the ion critical-gradient length and stiffness level and the impact of rotation in the JET tokamak*, PRL **102**, 175002 (2009)

[50] P. Strand, G. Bateman, A. Eriksson *et al*, 31th EPS conference London, UK, P5.187 (2004)

[51] G. M. Staeber, J. E. Kinsey and R. E. Waltz, *Gyro-Landau fluid equations for the trapped and passing particles*, Phys. Plasmas **12** 102508 (2005)

[52] G. Cennachi and A. Taroni, JETTO: Tech. Rep. JET-IR(88)03 JET Reports (1988)

[53] J. Weiland, *Collective Modes in Inhomogeneous Plasma*, Bristol: Institute of Physics Publishing (2000)

[54] T. Rafiq, A. H. Kritz, J. Weiland *et al*, *Physics basis of Multi-Mode anomalous transport module*, Phys. Plasmas **20** 032506 (2013)

[55] J. Nilsson and J. Weiland, *Fluid model for general collisionality and magnetic curvature*, Nucl. Fusion **34** 803 (1994)

[56] G. M. Staeber and J. E. Kinsey, *Electron collisions in the trapped gyro-Landau fluid model*, Phys. Plasmas **17** 122309 (2010)

[57] R. L. Miller, M. S. Chu, J. M. Green *et al*, *Noncircular, finite aspect ratio, local equilibrium model*, Phys. Plasmas **5**, 973-8 (1998)

[58] G. M. Staeber, J. Candy, N. T. Howard and C. Holland, *The role of zonal flows in the saturation of multi-scale gyrokinetic turbulence* Phys. Plasmas **23**, 062518 (2016)

[59] C. Angioni, F. Fable, M. Greenwald *et al*, *Particle transport in tokamak plasmas, theory and experiment*, Plasma Phys. Contr. F. **51**, 124017 (2009)

[60] H. Nordman J. Weiland and A. B. Jarmen, *Simulation of toroidal drift mode turbulence driven by temperature gradients and electron trapping*, Nucl. Fusion **30**, 983 (1990)

[61] E. Fable, C. Angioni, O. Sauter *The role of ion and electron electrostatic turbulence in characterizing stationary particle transport in the core of tokamak plasmas*, Plasma Phys. Contr. F. **52**, 015007 (2010)

[62] C. Angioni, R. M. McDermott, E. Fable *et al*, *Gyrokinetic modelling of electron and boron profiles of H-mode plasmas in ASDEX Upgrade*, Nucl. Fusion **51**, 023006 (2011)

[63] B. Baiocchi, C. Bourdelle, C. Angioni *et al*, *Transport analysis and modelling of the evolution of hollow density profiles in JET and implication for ITER*, Nucl. Fusion **55**, 123001 (2015)

[64] L. L. Lao, H. St.John, R. D. Stambaugh *et al*, *Reconstruction of current profile parameters and plasma shapes in tokamaks*, Nucl. Fusion **25**, 1611 (1985)

[65] C. D. Challis, J. G. Cordey, H. Hamnén *et al*, *Non-inductively driven currents in JET*, Nucl. Fusion **29** 563 (1989)

[66] W. A. Houlberg, K. C. Shaing, S. P. Hirshman *et al*, *Bootstrap cuurent and neoclassical transport in tokamaks of arbitrary collisionality and aspect ratio*, Phys. Plasmas **4**, 3230 (1997)

[67] T. H. Stix, *Fast-wave heating of a two-component plasma*, Nucl. Fusion **15** 737 (1975)

[68] P. Helander and D. J. Sigmar, *Collisional Transport in Magnetized Plasmas*, Cambridge University Press (2002)

[69] C. Estrada-Mila, J. Candy and R. E. Waltz, *Turbulent transport of alpha particles in reactor plasmas*, Phys. Plasmas **13**, 112303 (2006)

[70] F. Jenko and W. Dorland, *Nonlinear electromagnetic gyrokinetic simulations of tokamak plasmas*, Plasma Phys. Contr. F. 43 A141 (2001)

[71] A. Di. Siena, T. Görler, H. Doerk *et al*, *Non-Maxwellian fast particle effects in gyrokinetic GENE simulations*, Phys. Plasmas **25**, 042304 (2018)

[72] M. K. Lilley and R. M. Nyqvist, *Formation of phase space holes and clumps*, Phys. Rev. Lett. **112**, 155002 (2014)

[73] A. M Dimits, G. Bateman, M.A. Beer *et al*, *Comparisons and physics basis of tokamak transport models and turbulence simulations*, Phys. Plasmas **7**, 969-983 (2000)

[74] T. Tala, H. Nordman, A. Salmi *et al*, *Four separate dimensionless collisionality scans in various JET scenarious*, 44th EPS conference, Belfast, UK (2017)